Geochemistry, Geophysics, Geosystems®

RESEARCH ARTICLE
10.1029/2024GC011592

Key Points:

- Spatio-temporal rock uplift histories inferred from linear inversion of river profiled
- Impact of variable erodibility coefficient and downstream catchment lengthening on inversion results
- Quaternary uplift history of the Apennine belt and implications on the driving mechanisms

Supporting Information:

Supporting Information may be found in the online version of this article.

Correspondence to:

S. Racano,
racano@uni-potsdam.de

Citation:

Racano, S., van der Beek, P. A., Schildgen, T. F., Faccenna, C., Buleo Tebar, V., & Cosentino, D. (2024). Slab driven Quaternary rock-uplift and topographic evolution in the northern-central Apennines from linear inversion of the drainage system. *Geochemistry, Geophysics, Geosystems*, *25*, e2024GC011592. https://doi.org/10.1029/2024GC011592

Received 1 APR 2024
Accepted 8 JUL 2024

Author Contributions:

Conceptualization: S. Racano, P. A. van der Beek, T. F. Schildgen, C. Faccenna, D. Cosentino
Data curation: S. Racano
Formal analysis: S. Racano, V. Buleo Tebar
Investigation: S. Racano, C. Faccenna, D. Cosentino
Methodology: S. Racano, T. F. Schildgen, V. Buleo Tebar
Project administration: P. A. van der Beek
Resources: S. Racano, P. A. van der Beek
Software: S. Racano

Slab Driven Quaternary Rock-Uplift and Topographic Evolution in the Northern-Central Apennines From Linear Inversion of the Drainage System

S. Racano[1], P. A. van der Beek[1], T. F. Schildgen[1,2], C. Faccenna[2,3], V. Buleo Tebar[4], and D. Cosentino[3]

[1]Institute of Geosciences, University of Potsdam, Potsdam, Germany, [2]GFZ German Research Centre for Geosciences, Potsdam, Germany, [3]Department of Science, University of Roma Tre, Rome, Italy, [4]Department of Life Sciences and Systems Biology, University of Turin, Turin, Italy

Abstract Investigating rock-uplift variations in time and space provides insights into the processes driving mountain-belt evolution. The Apennine Mountains of Italy underwent substantial Quaternary rock uplift that shaped the present-day topography. Here, we present linear river-profile inversions for 28 catchments draining the eastern flank of the Northern-Central Apennines to reconstruct rock-uplift histories. We calibrated these results by estimating an erodibility coefficient (K) from incision rates and catchment-averaged erosion rates obtained from cosmogenic-nuclide data, and we tested whether a uniform or variable K produces a rock-uplift model that satisfactorily fits independent geochronological constraints. We employ a landscape-evolution model to demonstrate that our inversion results are reliable despite substantial seaward lengthening of the catchments during uplift. Our findings suggest that a rock-uplift pulse started around 3.0–2.5 Ma, coinciding with the onset of extension in the Apennines, and migrated southward at a rate of ∼90 km/Myr. The highest reconstructed rock-uplift rates (>1 km/Myr) occur in the region encompassing the highest Apennine massifs. These results are consistent with numerical models and field evidence from other regions exhibiting rapid rock-uplift pulses and uplift migration related to slab break-off. Our results support the hypothesis of break-off of the Adria slab under the central Apennines and its southward propagation during the Quaternary. Moreover, the results suggest a renewed increase in rock-uplift rates after the Middle Pleistocene along the Adriatic coast, coeval with recent uplift acceleration along the eastern coast of southern Italy in the Apulian foreland.

Plain Language Summary Rivers that drain mountainous regions store information on the history of mountain growth. Specifically, variations in the slope of rivers with distance can be interpreted as variations in the rate at which mountains grow through time. Because changes in slope may also occur due to changes in the hardness of rocks underlying the rivers, we must calibrate and correct our interpretations based on changes in rock type. We use 28 rivers draining the eastern flank of the Northern-Central Apennines of Italy to reconstruct temporal and spatial variations in the history of mountain growth. We find that a pulse of growth started between 3 and 2.5 million years ago and then migrated southwards through time. This southward movement is most likely associated with tectonic plate dynamics beneath the mountain belt, as the plate plunging beneath the Apennines tore progressively southward.

1. Introduction

The topography of mountain belts represents the result of large-scale and long-term interactions between crustal and mantle forces combined with climatic variations (e.g., Braun, 2010; Whipple, 2009; Wolf et al., 2022). Understanding the mechanisms driving the growth and evolution of topography in such settings is crucial for unraveling the dominant mountain-building processes, changes in the balance among these processes over time, and the tectonic history of mountain belts (e.g., Ballato et al., 2015; Faccenna et al., 2014; Gallen et al., 2023; Molin et al., 2012).

Numerous studies have probed the events that shaped the modern topography of the Apennine mountain chain, which runs along the length of the Italian Peninsula (e.g., Bartolini, 2003; Centamore & Nisio, 2003; Cosentino et al., 2010, 2017; Faccenna et al., 2014; Olivetti et al., 2012). While many authors have identified a rapid rock-uplift phase during the early Pleistocene (Cosentino et al., 2017; Fellin et al., 2021; Galadini et al., 2003) and strong coupling between rock-uplift and mantle processes (Cavinato & De Celles, 1999; D'Agostino et al., 2001;

Supervision: P. A. van der Beek, T. F. Schildgen
Validation: S. Racano, P. A. van der Beek, T. F. Schildgen, C. Faccenna, D. Cosentino
Visualization: S. Racano, T. F. Schildgen
Writing – original draft: S. Racano
Writing – review & editing: P. A. van der Beek, T. F. Schildgen, C. Faccenna, V. Buleo Tebar, D. Cosentino

Faccenna et al., 2014; Gvirtzman & Nur, 2001; Lanari et al., 2023; Picotti & Pazzaglia, 2008), there is no consensus on the relative importance of various tectonic and geodynamic mechanisms in building the Apennines. Those mechanisms include slab break-off (Faccenna et al., 2014; Faure Walker et al., 2012; Gvirtzman & Nur, 2001; Wortel & Spakman, 2000), mantle upwelling (D'Agostino et al., 2001), crustal delamination (Cavinato & De Celles, 1999), and orogenic wedge growth (Artoni, 2007). Currently active subduction beneath the outer arc of the northern Apennines and in the Calabrian Arc (Figure 1a) is evidenced by compressive earthquakes recorded along the outer margin of the chain as well as by the depressed dynamic topography that is likely linked to slab pull-down (Carminati et al., 2005, 2010; Diaferia et al., 2019; Faccenna & Becker, 2020; Faccenna et al., 2014). This inference is further supported by regional subsidence estimates derived from GPS data (Carminati et al., 2005; Faccenna et al., 2014). In contrast, the central and southern Apennines are dominated by extensional tectonics and lack the signature of processes associated with active subduction (Faccenna & Becker, 2020; Faccenna et al., 2014; Serpelloni et al., 2013). Additionally, geophysical studies have revealed positive residual topography in these regions, which is not compensated by a crustal root (Faccenna & Becker, 2020; Faccenna et al., 2014).

The study of geomorphic features, particularly the analysis of drainage systems, offers critical insights into the topographic evolution of a region (e.g., Pavano & Gallen, 2021; Schildgen et al., 2012; Siravo et al., 2021). Characteristics such as river-incision rates, river steepness, knickpoints, and divide stability are valuable tools for quantifying temporal and spatial variations in rock uplift and/or erosion, assessing their impact on topography, and determining the driving forces shaping the landscape (e.g., Buleo Tebar et al., 2024; Clementucci et al., 2023; Gallen et al., 2023; Pavano et al., 2024; Racano et al., 2021, 2023).

Here, we explore the Quaternary spatiotemporal evolution of rock uplift along the Northern and Central Apennines by linear inversion of river profiles (Gallen, 2018; Goren et al., 2014). We focus our study on rivers draining the outer Adriatic flank of the chain (Figure 1b), which flow nearly perpendicular to the strike of the mountain belt and show little evidence of integration with intra-montane basins and variations in divide position over the last few Myr (Lanari et al., 2023). To calibrate the river-profile inversions and determine the temporal time frame of rock-uplift variations, we quantify the erodibility coefficient using a combination of published terrestrial cosmogenic nuclide denudation rates and river-incision rates derived from dated strath terraces and paleosurfaces in these catchments. Because the study area experienced coastal uplift and subsequent downstream expansion of catchments since the Middle Pleistocene (Centamore & Nisio, 2003; Centamore & Rossi, 2009), we perform Landscape Evolution Model (LEM) simulations to explore the impact of fluvial lengthening on the river-profile inversion results. Finally, we combine the inferred rock-uplift histories from individual catchments to develop an uplift model describing the spatio-temporal variations in rock uplift along the eastern flank of the Northern and Central Apennines and discuss the probable tectonic and geodynamic processes driving this uplift.

2. Geological Background

The Apennine mountain belt (Figure 1) is the result of multi-phase tectonics that started during the late Oligocene-early Miocene with the activation of thrust faults that propagated eastward, following the late stages of subduction and slab roll-back of the Adria plate (e.g., Cosentino et al., 2010; Di Giulio et al., 2013; Faccenna et al., 2007; Royden et al., 1987). During the late Pliocene to early Pleistocene, the Apennines experienced a change in the dominant tectonic regime, shifting from compressional to extensional deformation. Pleistocene extension is mainly expressed along SW-dipping normal faults, which cause local range uplift and opening of intra-montane basins (e.g., Cavinato & De Celles, 1999; Cosentino et al., 2017; D'Agostino et al., 2001, 2011). The onset of normal faulting follows a north-eastward younging trend in the Northern Apennines (Collettini & Barchi, 2004; Collettini et al., 2006; Cosentino et al., 2010; Patacca et al., 1993). In the Central Apennines, in contrast, normal faults initiated almost synchronously at about 2.5 Ma (Cosentino et al., 2017).

The present topography of the Apennines is closely linked to mantle dynamics and active subduction, where it still occurs (Faccenna & Becker, 2020; Lanari et al., 2023). In the Northern Apennines (Figure 1b), south-westward capture of intra-montane basins during the Plio-Pleistocene has been linked to the progressive eastward migration of an extensional retro-wedge and compressional pro-wedge system, driven by subduction and slab rollback (Lanari et al., 2023) or delamination-retreat of the subducting plate (Chiarabba et al., 2014). The presence of a shallow (approximately 30-km deep) subduction interface is confirmed by seismic tomography and compressive earthquakes recorded on the outer front of the chain (Boccaletti et al., 2011; Eva et al., 2005; Faccenna

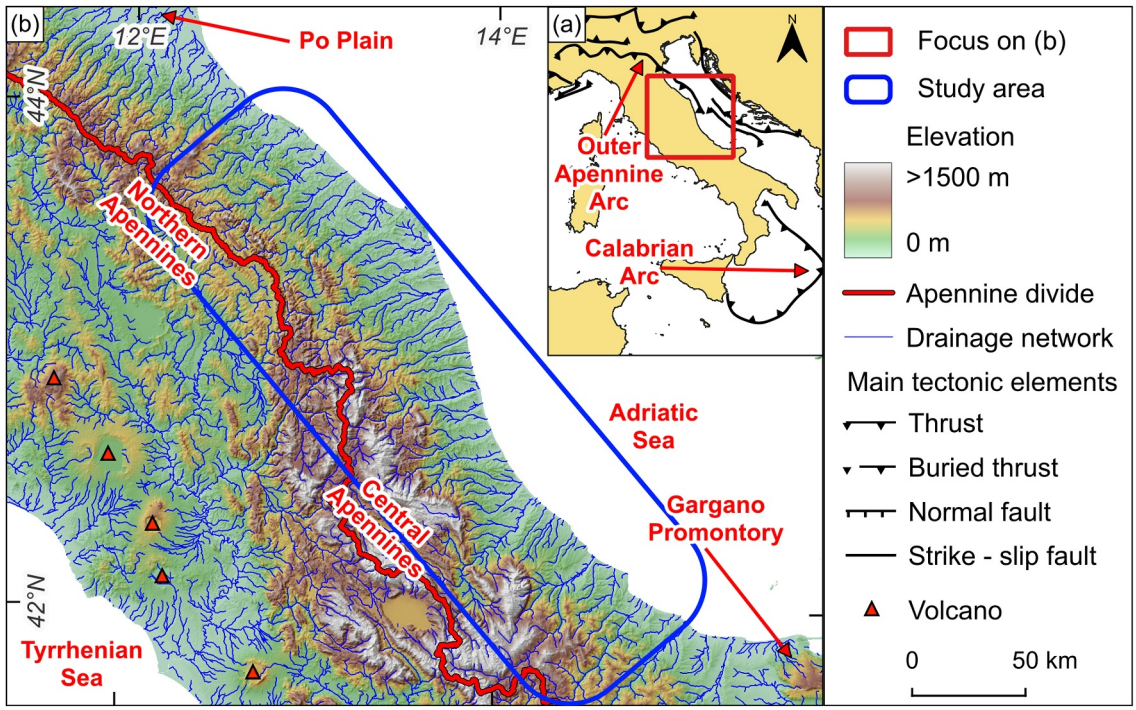

Figure 1. (a) Regional tectonic setting of the Apennines. Inset shows location of (b); (b) Digital elevation model of central Italy, showing location of the study area, principal regional topographic elements, drainage patterns, and trace of the main Apennine drainage divide.

et al., 2014). Along the Calabrian Arc (Figure 1a), seismic tomography and deep compressional earthquakes (at depths greater than 300 km) also suggest the presence of a subducting slab (Chiarabba et al., 2005; Faccenna et al., 2014). In the Central and Southern Apennines, in contrast, the absence of deep seismicity, the overall extensional tectonic regime, and the shallow depth of the Moho indicate that the topography is supported by mantle upwelling through slab windows (Chiarabba et al., 2020). Mantle upwelling has been argued to be linked to slab break-off (Faccenna et al., 2014; Lanari et al., 2023) or to segmentation and differential slab retreat among the northern, central-southern, and Calabrian segments of the Adria Plate (Scrocca, 2006).

Thermochronological and geochemical studies provide evidence for the recent rapid uplift in the Central Apennines. Apatite fission track and (U-Th)/He cooling ages in the Central Apennines reveal that the most recent exhumation phase began at approximately 2.5 Ma, coinciding with the onset of normal faulting and the opening of intra-montane basins throughout the Central Apennines (Cosentino et al., 2017; Fellin et al., 2021). Stable oxygen-isotope ($\delta^{18}O$) data from intra-montane lacustrine sediments and paleosols similarly indicate a rapid increase in elevation after the late Pliocene (San Jose et al., 2020).

The Apennine divide marks the boundary between two sectors, the Tyrrhenian to the west and the Adriatic to the east (Figure 1b), which have substantially different Quaternary geological histories. Within the Tyrrhenian sector, normal faulting along the coastal region since the late Miocene (Carmignani et al., 1994), together with Quaternary volcanism, caused regional drainage reorganization (Funiciello et al., 2003; Tentori et al., 2016) and eastward drainage-divide migration due to the change from endorheic to exoreic conditions of several intra-Apennine basins (Lanari et al., 2023). Modern regional drainage directions in the Tyrrhenian sector are mainly parallel to the Apennine axis or radial around the volcanic edifices (Figure 1b). In comparison with the Tyrrhenian sector, the Adriatic sector has experienced a simpler tectonic history with apparently more stable conditions along the regional divide. Except for the Aterno-Pescara River, which mainly flows NW–SE following the direction of the intra-montane basins (Figure 2), the general drainage direction in the Adriatic sector is SW–NE to WSW–ENE, following the regional topographic slope and overall monoclinal structure (Buccolini et al., 2010; Figure 1b). While the inner Apennine chain in the Adriatic sector shows indications of early Pleistocene rock uplift, the coastal region (known as the peri-Adriatic belt) only experienced rock uplift from the early Middle Pleistocene onward (Centamore & Nisio, 2003; Centamore & Rossi, 2009). Uplift rates in the peri-Adriatic belt

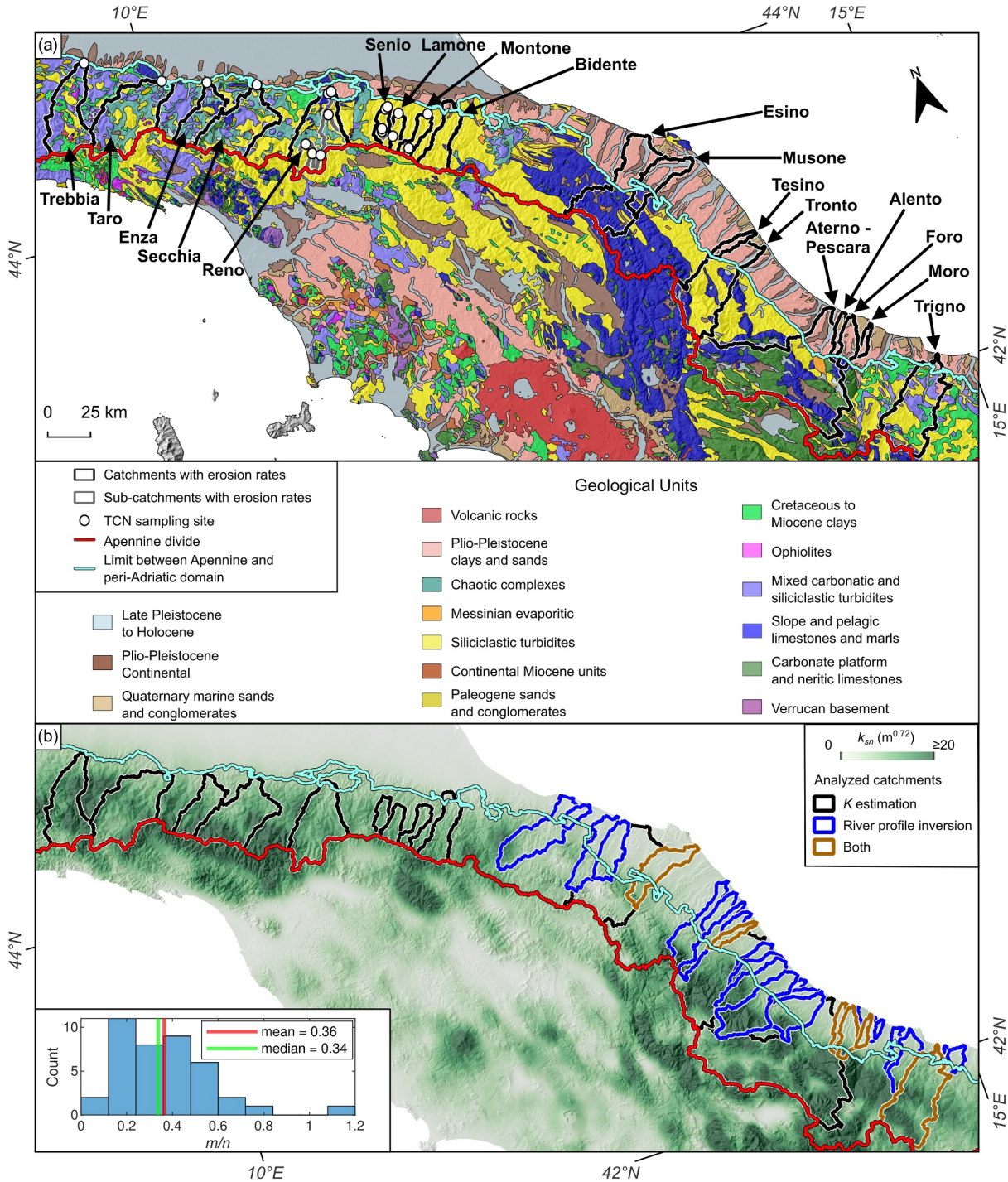

Figure 2. (a) Geological map of the Northern and Central Apennines showing the main geological units and the catchments used to estimate the erosional efficiency parameter *K*. The map is modified from the 1:500,000-scale Geological Map of Italy, available from the Italian National Geoportal (http://sgi2.isprambiente.it/arcgis/services/servizi/cartageologica500k/MapServer/WmsServer); White diamonds indicate terrestrial cosmogenic nuclide sampling sites for catchment-wide erosion-rate measurements; in catchments without diamonds, local incision rates were measured from dated terraces. (b) Interpolated k_{sn} map of the Northern and Central Apennines, showing catchments used to estimate *K* and catchments on which river-profile inversion was applied. Inset shows histogram of best-fit concavity index (*m*/*n*) for all selected catchments, with mean and median values.

appear to have remained constant since the Middle Pleistocene (Cyr & Granger, 2008; Delchiaro et al., 2024; Sembroni et al., 2020), producing a steep coast that reaches a maximum elevation of 100 m a.s.l., characterized by fluvially incised Plio-Pleistocene marine successions.

3. Methods

3.1. Stream-Power Law and Drainage Metrics

For rivers incising bedrock, the spatial and temporal evolution of the bed elevation with respect to baselevel, $z(t, x)$, is determined by the balance between rock uplift and river incision (Whipple & Tucker, 1999):

$$\frac{dz(t,x)}{dt} = U(t,x) - E(t,x) \tag{1}$$

where $U(t, x)$ is the rock-uplift rate, and $E(t, x)$ is the incision rate, which, for detachment-limited rivers, can be described by the stream-power law:

$$E(t,x) = KA(x)^m S(t,x)^n \tag{2}$$

where A is the upstream drainage area, S is the channel slope, K is an erodibility coefficient, which is primarily related to geology and climate, and m and n are two positive constants related to basin hydrology and channel-erosion processes, respectively (Howard, 1994; Whipple & Tucker, 1999).

Solving for channel slope in Equation 2 yields:

$$S = \left(\frac{E}{K}\right)^{\frac{1}{n}} A^{-\frac{m}{n}} \tag{3}$$

For steady-state conditions ($E = U$) and spatially and temporally uniform K, Equation 3 can be integrated to predict the bed elevation along the river profile (Perron & Royden, 2013):

$$z(x) = z(x_b) + \left(\frac{U}{KA_0^m}\right)^{\frac{1}{n}} \chi \tag{4}$$

where $z(x_b)$ is the elevation of the catchment outlet, A_0 is a reference drainage area, and χ is an integral of the horizontal coordinates calculated from the outlet x_b to a given point x and dependent on A:

$$\chi(x) = \int_{x_b}^{x} \left(\frac{A_0}{A(x')}\right)^{\frac{m}{n}} dx' \tag{5}$$

By setting the reference area A_0 equal to 1, the slope of the plot defined by Equation 4 is equivalent to the river steepness index (Smith et al., 2022), which can be defined from Equation 3 under steady-state conditions:

$$k_s = \left(\frac{U}{K}\right)^{\frac{1}{n}} = S(x)A(x)^{\frac{m}{n}} \tag{6}$$

The ratio m/n defines the concavity index. By applying a uniform m/n to a regional drainage system, we obtain the normalized steepness index (k_{sn}), which is a robust measure of relative channel steepness throughout a region (Wobus et al., 2006) and, for $n = 1$ and block-uplift conditions, can be considered a nondimensional proxy of the rock-uplift history recorded in drainage systems (Pavano & Gallen, 2021; Racano et al., 2023). We estimate an average m/n ratio for the outer flank of the Apennines by minimizing the scatter in resulting χ–z plots following Goren et al. (2014; Figure 2b).

3.2. Rock-Uplift Histories From Linear Inversion of River Profiles

Linear inversions of river profiles have been used to extract temporal (e.g., Gallen, 2018; Gallen et al., 2023; Goren et al., 2014; Pritchard et al., 2009) or spatiotemporal (e.g., Fox et al., 2015; McNab et al., 2018; Quye-Sawyer et al., 2020) variations in rock-uplift histories. While the latter approaches have usually been applied

at regional to continental scales, the former approaches assume spatially uniform rock uplift and can be a useful and computationally efficient way to invert river profiles locally, such as for a single catchment. The results from several individually inverted catchments can then be combined to estimate spatiotemporal variations in rock-uplift histories (e.g., Pavano & Gallen, 2021; Racano et al., 2021, 2023; Zhong et al., 2022).

For $n = 1$ and block-uplift conditions, Goren et al. (2014) developed a linear inversion approach, whereby the rock-uplift history is obtained by a least-square solution of Equation 4 organized in matrix form, assuming that every part of the drainage system that has the same χ value records the same rock-uplift history. A non-dimensional rock-uplift term (U^*) is inferred by averaging the gradient of χ-plots for chosen χ intervals. Specifically,

$$z = \boldsymbol{A}^* U^* \tag{7}$$

$$U^* = U^*_{\text{pri}} + \left(\boldsymbol{A}^{*T}\boldsymbol{A}^* + \Gamma^2 \boldsymbol{I}\right)^{-1} \boldsymbol{A}^{*T}\left(z - \boldsymbol{A}^* U^*_{\text{pri}}\right) \tag{8}$$

where $\boldsymbol{A}^*$ is an $N \times q$ matrix (with N the number of data points and q the number of χ intervals), Γ is a dampening coefficient that determines the smoothness imposed on the solution, $\boldsymbol{I}$ is the $q \times q$ identity matrix and U^*_{pri} represents the prior guess for U^*, usually taken as the average slope of the χ-plot (Goren et al., 2014).

χ and U^* can be converted to real time and rock-uplift rates, respectively, by the following equations:

$$\tau = \frac{\chi}{K A_0^m} \tag{9}$$

$$U = U^* K A_0^m \tag{10}$$

τ represents the travel time of a perturbation along a river profile from the outlet ($x = 0$) to a given channel distance x (Goren et al., 2014; Whipple & Tucker, 1999). Taking the same conditions as those applied for non-dimensional linear river-profile inversion, τ can be defined by the integral:

$$\tau(x) = \int_0^x \frac{dx}{K(x) A(x)^m} \tag{11}$$

and can be used to predict the shape of a river profile by the equation:

$$z(x) = \int_{-\tau}^{0} U(t)\, dt \tag{12}$$

where 0 is the present time and $-\tau$ represents the onset time of the tectonic history recorded by a point x in the catchment. Equation 12 is the base of the approach developed by Gallen (2018) to derive rock-uplift histories. For this method, K must be known a priori to infer τ from Equation 9, after which the same inversion approach as that of Goren et al. (2014) (Equations 7 and 8) can be applied to the river profile in z-τ space to derive U from chosen τ increments. The main difference with the non-dimensional approach is that the estimation of τ can be made taking into account a spatial variable, such as a lithology-dependent K (Fisher, Pazzaglia, et al., 2022; Gallen, 2018; Pazzaglia & Fisher, 2022) instead of using an average K for the inverted catchment to convert U^* and χ to U and τ. Thus, the approach developed by Gallen (2018) allows imposing more geologically informed constraints on uplift-rate variations in cases where K varies substantially along a river.

3.3. Application to the Adriatic Flank of the Apennines

One limitation of the variable-K approach is that it considers the position of the lithological boundaries to be fixed through time, whereas in reality, their positions depend on the geometry and orientation of lithologic contacts, which can move over time as the landscape erodes. In addition, K is sensitive to topographic and climatic features,

which are not included when K is estimated only from lithology. Considering this issue, we divided the study area into two distinct geological domains, taking into account not only the outcropping lithologies but also the topographic characteristics: (a) the Apennine domain, consisting mainly of pre- and syn-orogenic lithologic successions and characterized by high elevations and relief; and (b) the peri-Adriatic domain, the hilly coastal belt primarily composed of Plio-Pleistocene (mainly late- and post-orogenic) coastal successions and a few (pre-orogenic) bedrock outcrops in the northern part of the belt (Figure 2a). The limit between these domains can be considered mostly stable over time, as no significant shortening has affected the region during the Quaternary uplift phase (Pizzi, 2003), allowing us to calculate τ with a K value that varies between these geologically defined domains. In this classification, we disregard climatic differences (e.g., average annual precipitation), as they have a lesser influence on fluvial indices (i.e., steepness index k_{sn}, erodibility coefficient K) than topographic parameters such as relief or slope (Figures S1 and S2 in Supporting Information S1).

To infer the regional rock-uplift history, we selected 28 river catchments, spanning from the Po Plain in the north to the Gargano Promontory in the south (Figures 1 and 2). We subsequently integrated the results from each catchment to derive a spatiotemporal model of rock uplift, following the approach of Racano et al. (2021, 2023). We focused on catchments draining only the eastern flank of the Apennine belt to avoid complications due to Quaternary normal faulting and the opening of intra-montane basins, drainage reorganization and divide migration within the inner chain, and volcanic activity on the Tyrrhenian flank (Funiciello et al., 2003; Lanari et al., 2023; Tentori et al., 2016). The drainage system and catchments were extracted using TopoToolbox (Schwanghart & Scherler, 2014) based on topography from the COPERNICUS 30-m resolution Digital elevation model and a minimum upstream drainage area of 1 km^2.

Assuming $n = 1$, and substituting E for U (which can be done if local erosion rate balances the rock-uplift rate), K can be estimated from Equation 6:

$$K = \frac{E}{k_{sn}} \tag{13}$$

E can be derived from catchment-average denudation rates (e.g., Clementucci et al., 2023; Fisher, Pazzaglia, et al., 2022; Racano et al., 2023), incision rates of dated landforms (Pazzaglia & Fisher, 2022), or long-term exhumation rates from thermochronology (Gallen et al., 2023; Glotzbach, 2015). Alternatively, for coastal rivers, U can be derived from dated uplifted marine terraces (Gallen et al., 2023; Racano et al., 2021) and used instead of E in Equation 13. In individual catchments, K can be estimated by dividing individual estimates of E or U by k_{sn}. At a regional scale, K can be determined from a linear regression between k_{sn} and E or U, as K represents the slope of Equation 6. We utilized data from 18 catchments along the northern (draining to the Po Plain) and Adriatic (draining directly to the sea) flanks of the Apennines (Figure 2), for which we compiled literature data on catchment-average denudation rates (Cyr et al., 2014; Wittmann et al., 2016), river-incision rates from dated fluvial strath terraces and paleosurfaces (Amato et al., 2017; Crescenti et al., 2015; Delchiaro et al., 2024; Sembroni et al., 2020; Wegmann & Pazzaglia, 2009), and rock-uplift rates from leveling studies (D'Anastasio et al., 2006) (Table 1), river-incision rates from dated fluvial strath terraces and paleosurfaces, and rock-uplift rates from leveling studies (Table 1). Local incision rates from strath terraces are mainly available for the peri-Adriatic sector of these catchments. In our analysis, we assume that these incision rates can be extrapolated to the entire catchments (both the Apennine and peri-Adriatic domains); in other words, we assume that these catchments are approximately in a steady state (Cyr & Granger, 2008). We estimated the average K-value of the selected catchments as well as K-values representative of the Apennine and peri-Adriatic domains to apply river-profile inversion accounting for both constant and spatially variable erodibility using a modified version of the code developed by Pazzaglia and Fisher (2022). We employed an arbitrary τ increment of 200 kyr for the reconstructed rock-uplift histories. For shorter rivers, where the 200 kyr increment was too large, we used a smaller increment of 100 kyr. Finally, we combined the results using a LOWESS linear smoothing function from the MATLAB® Curve Fitting Toolbox to generate a spatiotemporal model of rock uplift.

3.4. Testing the Impact of Seaward Catchment Lengthening on River-Profile Inversion

The linear river-profile inversion approach used to infer rock-uplift histories from river profiles assumes a (near-) steady-state catchment geometry over the investigated time. This implies that changes in drainage area, as might occur through drainage capture, for instance, may alter the inferred rock-uplift history. When a river captures (part

Geochemistry, Geophysics, Geosystems

10.1029/2024GC011592

Table 1
Erosion Rates, k_{sn}, and K Estimation for the Catchments Used to Calibrate River-Profile Inversions

					(1) Catchment average (m/n = 0.36)				(2) Apennine domain (m/n = 0.36)				(3) peri-Adriatic domain (m/n = 0.36)			
Catchment	Reference	Method	E mean	E err	k_{sn} mean	k_{sn} std	K mean	K err	k_{sn} mean	k_{sn} std	K mean	K err	k_{sn} mean	k_{sn} std	K mean	K err
Trebbia	Wittmann et al. (2016)	TCN catchment average denudation rate	0.44	0.02	17.05	4.96	2.6×10^{-5}	8.2×10^{-6}	same as (1)	same as (1)	same as (1)	same as (1)	n/a	n/a	n/a	n/a
Taro	Wittmann et al. (2016)	TCN catchment average denudation rate	0.61	0.02	14.21	3.96	4.3×10^{-5}	1.2×10^{-5}	same as (1)	same as (1)	same as (1)	same as (1)	n/a	n/a	n/a	n/a
Enza	Wittmann et al. (2016)	TCN catchment average denudation rate	0.5	0.02	14.87	4.79	3.4×10^{-5}	1.1×10^{-5}	same as (1)	same as (1)	same as (1)	same as (1)	n/a	n/a	n/a	n/a
Vispa	Wittmann et al. (2016)	TCN catchment average denudation rate	0.65	0.03	16.57	6.17	3.9×10^{-5}	1.5×10^{-5}	same as (1)	same as (1)	same as (1)	same as (1)	n/a	n/a	n/a	n/a
Reno	Cyr et al. (2014)	TCN catchment average denudation rate	0.35	0.09	7.5	0.65	4.7×10^{-5}	1.3×10^{-5}	same as (1)	same as (1)	same as (1)	same as (1)	n/a	n/a	n/a	n/a
Reno at Fontana		TCN catchment average denudation rate	0.57	0.15	14.08	3.22	4.1×10^{-5}	1.4×10^{-5}	same as (1)	same as (1)	same as (1)	same as (1)	n/a	n/a	n/a	n/a
Setta at Piccolo Paradiso		TCN catchment average denudation rate	0.85	0.39	10.56	2.87	8.1×10^{-5}	4.3×10^{-5}	same as (1)	same as (1)	same as (1)	same as (1)	n/a	n/a	n/a	n/a
Sambro at Rioveggio		TCN catchment average denudation rate	0.56	0.15	14.24	2.03	3.9×10^{-5}	1.2×10^{-5}	same as (1)	same as (1)	same as (1)	same as (1)	n/a	n/a	n/a	n/a
Reno at Poretta Terme		TCN catchment average denudation rate	0.22	0.05	15.08	2.23	1.5×10^{-5}	3.8×10^{-6}	same as (1)	same as (1)	same as (1)	same as (1)	n/a	n/a	n/a	n/a
Limentra di Samb. at Taviano		TCN catchment average denudation rate	0.2	0.04	11.92	0.72	1.7×10^{-5}	3.9×10^{-6}	same as (1)	same as (1)	same as (1)	same as (1)	n/a	n/a	n/a	n/a
Limetrella di Treppio at Treppio		TCN catchment average denudation rate	0.19	0.04	11.73	0.56	1.6×10^{-5}	2.7×10^{-6}	same as (1)	same as (1)	same as (1)	same as (1)	n/a	n/a	n/a	n/a
Senio (at Casola Valsenio – A)	Cyr et al. (2014)	TCN catchment average denudation rate	0.3	0.07	11.9	0.63	2.5×10^{-5}	6.1×10^{-6}	same as (1)	same as (1)	same as (1)	same as (1)	n/a	n/a	n/a	n/a
Senio (at Casola Valsenio – B)		TCN catchment average denudation rate	0.48	0.13	11.9	0.63	4.1×10^{-5}	1.1×10^{-5}	same as (1)	same as (1)	same as (1)	same as (1)	n/a	n/a	n/a	n/a
Senio at Palazzuolo		TCN catchment average denudation rate	0.36	0.1	14.38	1.31	2.5×10^{-5}	7.1×10^{-6}	same as (1)	same as (1)	same as (1)	same as (1)	n/a	n/a	n/a	n/a
Visano at Palazzuolo		TCN catchment average denudation rate	0.32	0.07	12.46	0.31	2.5×10^{-5}	5.8×10^{-6}	same as (1)	same as (1)	same as (1)	same as (1)	n/a	n/a	n/a	n/a
Lamone (at San Eufemia)	Cyr et al. (2014)	TCN catchment average denudation rate	0.31	0.07	12.71	1.98	2.4×10^{-5}	6.1×10^{-6}	same as (1)	same as (1)	same as (1)	same as (1)	n/a	n/a	n/a	n/a
Lamone at Biforco		TCN catchment average denudation rate	0.3	0.06	14.46	1.72	2.1×10^{-5}	4.9×10^{-6}	same as (1)	same as (1)	same as (1)	same as (1)	n/a	n/a	n/a	n/a

Geochemistry, Geophysics, Geosystems

10.1029/2024GC011592

Table 1
Continued

Catchment	Reference	Method	E mean	E err	(1) Catchment average (m/n = 0.36) k_{sn} mean	k_{sn} std	K mean	K err	(2) Apennine domain (m/n = 0.36) k_{sn} mean	k_{sn} std	K mean	K err	(3) peri-Adriatic domain (m/n = 0.36) k_{sn} mean	k_{sn} std	K mean	K err
Montone (at Davadola)	Cyr et al. (2014)	TCN catchment average denudation rate	0.58	0.15	11.26	2.47	5.1×10^{-5}	1.7×10^{-5}	same as (1)	same as (1)	same as (1)	same as (1)	n/a	n/a	n/a	n/a
Montone at San Benedetto		TCN catchment average denudation rate	0.37	0.1	14.3	0.22	2.6×10^{-5}	6.9×10^{-6}	same as (1)	same as (1)	same as (1)	same as (1)	n/a	n/a	n/a	n/a
Bidente	Wegmann and Pazzaglia (2009)	Paleosurface and strath terrace incision rates	1.3	0.13	11.54	3.2	1.1×10^{-4}	3.3×10^{-5}	12.07	2.77	1.1×10^{-4}	3.1×10^{-5}	5.68	1.04	2.3×10^{-4}	4.8×10^{-5}
Esino	D'Anastasio et al. (2006)	Geodetic releveling	0.54	0.05	6.26	3.54	8.6×10^{-5}	4.9×10^{-5}	7.8	3.29	6.9×10^{-5}	2.8×10^{-5}	3.99	2.55	1.4×10^{-4}	8.7×10^{-5}
Musone	Wegmann and Pazzaglia (2009)	Paleosurface and strath terrace incision rates	0.55	0.03	6.13	3.99	9.1×10^{-5}	5.9×10^{-5}	11.62	2.33	4.7×10^{-5}	7.9×10^{-6}	3.82	1.78	1.4×10^{-4}	6.8×10^{-5}
Tesino	Delchiaro et al. (2024)	Paleosurface and strath terrace incision rates	0.32	0.05	7.05	1.21	4.5×10^{-5}	9.9×10^{-6}	n/a	n/a	n/a	n/a	7.05	1.22	4.5×10^{-5}	9.6×10^{-6}
Tronto	Sembroni et al. (2020)	Paleosurface and strath terrace incision rates	0.6	0.03	16.27	7.78	3.7×10^{-5}	1.8×10^{-5}	18.54	6.71	3.2×10^{-5}	1.5×10^{-5}	6.57	1.33	1.1×10^{-4}	2.3×10^{-5}
Aterno-Pescara	Crescenti et al. (2015)	Paleosurface and strath terrace incision rates	1.03	0.07	17.87	7.73	5.8×10^{-5}	2.9×10^{-5}	19.13	7.14	5.4×10^{-5}	2.1×10^{-5}	7.42	3.28	1.4×10^{-4}	7.2×10^{-5}
Alento	Crescenti et al. (2015)	Paleosurface and strath terrace incision rates	0.85	0.12	8.61	6.62	9.9×10^{-5}	9.1×10^{-5}	22.46	2.11	3.8×10^{-5}	5.7×10^{-6}	6.53	4.07	1.3×10^{-4}	9.8×10^{-5}
Foro	Crescenti et al. (2015)	Paleosurface and strath terrace incision rates	0.88	0.1	9.94	7.31	8.9×10^{-5}	6.5×10^{-5}	26.67	3.88	3.3×10^{-5}	5.7×10^{-6}	7.64	3.85	1.2×10^{-4}	5.9×10^{-5}
Moro	Crescenti et al. (2015)	Paleosurface and strath terrace incision rates	1.21	0.13	5.34	0.58	2.1×10^{-4}	1.9×10^{-5}	n/a	n/a	n/a	n/a	5.34	0.57	2.3×10^{-4}	5.3×10^{-5}
Trigno	Amato et al. (2017)	Paleosurface and strath terrace incision rates	0.85	0.47	14.75	4.59	5.8×10^{-5}	2.1×10^{-5}	15.12	4.26	5.6×10^{-5}	1.5×10^{-5}	5.32	1.3	1.6×10^{-4}	4.8×10^{-5}

Note. Denudation rates are from the OCTOPUS V2 database (Codilean et al., 2022); values have been recalculated by using the CAIRN method (Mudd et al., 2016).

of) an adjacent drainage basin, the increase in drainage area leads to upstream lengthening of stream channels (Figure S3 in Supporting Information S1). Equations 5 and 11 show that the upstream drainage area is inversely proportional to both χ and τ, implying that if a catchment captures a new area, both χ and τ will decrease (i.e., the response time at any given point in the original catchment will be shorter after capture).

Although the upstream boundary of the Adriatic catchments (i.e., the main Apennine drainage divide) can be considered relatively stable over the last 3 Myr (Lanari et al., 2023), the uplift affecting the peri-Adriatic belt during the Middle Pleistocene (Centamore & Nisio, 2003; Centamore & Rossi, 2009) resulted in seaward lengthening of catchments by up to 30 km (Figure S4 in Supporting Information S1) and a downstream increase in drainage area. Racano et al. (2021) argued that for very rapid uplift rates (up to 3.5 km/Myr) and steep offshore bathymetry, the coastward lengthening of catchments probably has a limited impact on τ and, consequently, on rock-uplift histories inferred from river-profile inversion. However, whereas the effect of adding upstream drainage area through capture has been the focus of several recent studies (e.g., Giachetta & Willett, 2018; Gong et al., 2024; Rohrmann et al., 2023), to our knowledge, the effects of downstream lengthening have not been directly tested.

To test the effect of seaward lengthening of river profiles on uplift histories derived from river-profile inversions, we ran a LEM that combines rock uplift and coastal migration over time. Using the TTLEM (TopoToolbox LEM; Campforts et al., 2017), we developed a scenario accounting for spatially variable K, temporally variable uplift, and downstream drainage lengthening over time. The initial setup is represented by a 60 × 30 km flat region, divided into two areas with different K values, representative of the average erodibilities for the Apennine and the peri-Adriatic domains (see below). Rivers are forced to flow only in one direction, from the inland to the coastal areas, by imposing closed northern, eastern and southern boundaries. Starting from the same initial landscape, we performed simulations that (a) uplift the entire landscape for the entire 5-Myr simulation time, (b) progressively lengthen the coastal belt by 7.5 km every 250 kyr starting from 4 Myr, and (c) suddenly lengthen the coastal belt after 4 Myr. For each simulation, we extracted the main trunk streams and performed river-profile inversions on these for both constant K (using an average value for K between coastal and inland areas) and variable K to study how well the inferred rock-uplift history reproduces the input uplift rates (Movies S1–S3). The detailed setup of the LEMs and parameter values are provided in Table S3.

4. Results

4.1. Determining the Erodibility Coefficient K in the Apennine and the peri-Adriatic Domains

^{10}Be derived denudation rates in the northern catchments (Trebbia to Bidente; draining into the Po Plain) range from 0.19 to 0.65 km/Myr (Table 1); rates are generally higher in catchments dominated by mixed carbonate and siliciclastic rocks than in those dominated by siliciclastic turbidites (Figure 3a). In the Adriatic catchments (Esino to Foro), incision rates from strath terraces and paleosurfaces are mostly available for the peri-Adriatic domain, and for only two catchments draining the Apennine domain (Bidente, draining to the Po Plain, and Trigno, draining to the Adriatic See; Figure 2, Table 2). These rates exhibit higher variability (0.32–1.3 km/Myr, Tables 1 and 2) and tend to increase toward the south (Figure 3a).

The average m/n ratio estimated for all the analyzed catchments is 0.36 (Figure 2b), similar to the catchments draining the westernmost part of the Northern Apennines (Buleo Tebar et al., 2024). Applying this value to calculate k_{sn}, the average k_{sn} values for the northern catchments exhibit a slightly eastward-decreasing trend (Figure 3b). In the western catchments (from the Trebbia to the Reno), which are dominated by mixed carbonate and siliciclastic rocks, k_{sn} values are higher than those in the eastern Senio, Lamone, Montone, and Bidente catchments, where the dominant lithologies are siliciclastic turbidites. The catchment-average k_{sn} values for the Adriatic catchments show high variability, similar to the incision rates, particularly when considering the average k_{sn} values for the full catchments (Figure 3b). However, when separating the Apennine and peri-Adriatic belts within the Adriatic catchments (Figure 3c), the k_{sn} values for the Apennine domain (comprising limestones, marls, and siliciclastic turbidites) show a lower standard deviation and a bell-shaped trend, with the highest values recorded in the central Tronto, Aterno-Pescara, and Alento catchments. The k_{sn} values for the peri-Adriatic domain (comprising clays, sandy clays, sands, and conglomerates) are substantially lower than the catchment-average k_{sn} values and show much less variability.

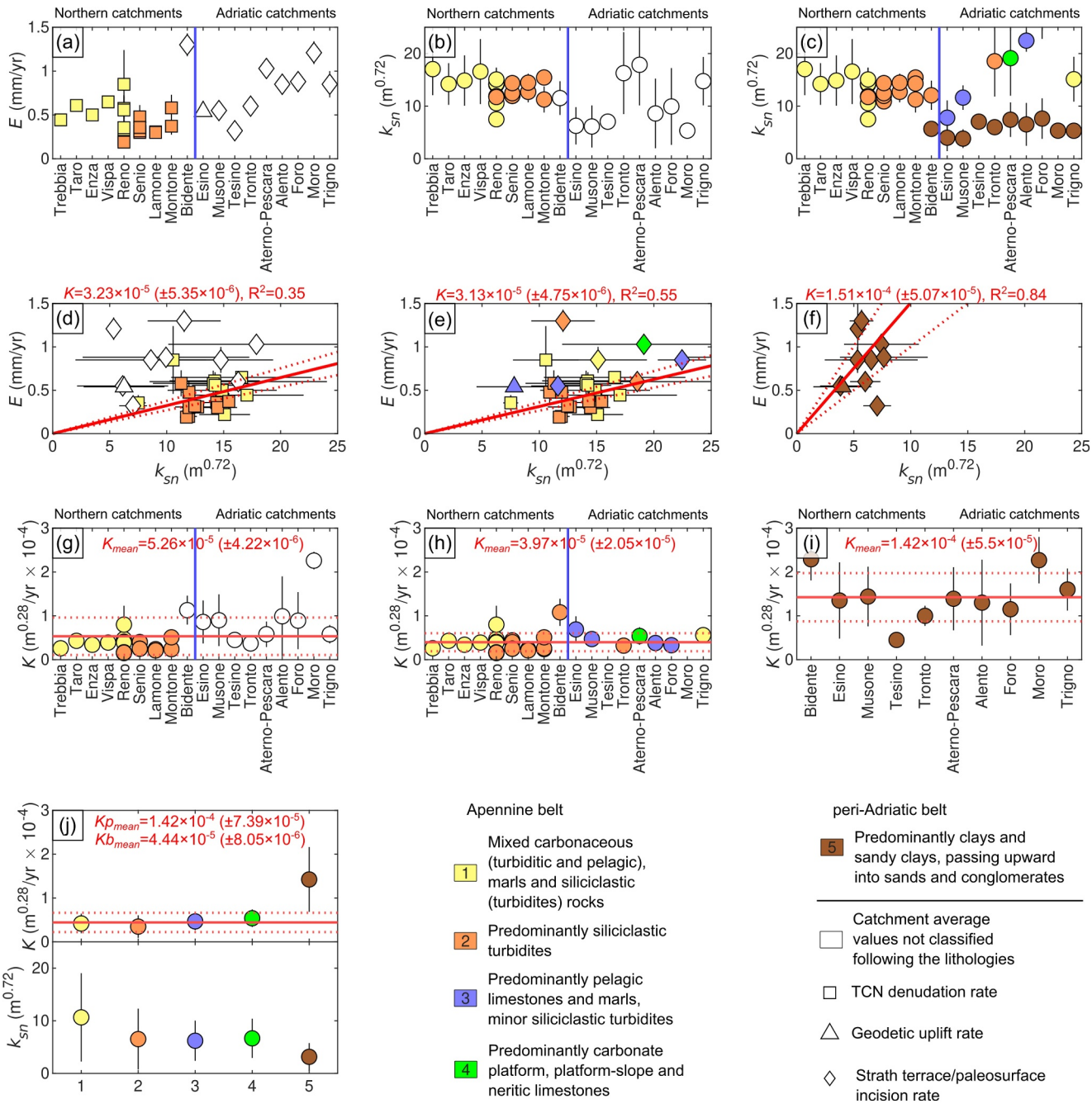

Figure 3. (a) Average denudation, incision, and geodetic uplift rates (E), and (b and c) average normalized steepness index (k_{sn}) in the catchments used to infer K along the outer flank of the northern-central Apennines (data sources shown in Table 1). Squares indicate TCN-derived average catchment denudation rates; diamonds and triangles refer to catchments for which we used strath terrace incision rate and uplift rate from geodetic measurements. The blue line separates catchments draining to the Po Plain (to the left) from Adriatic catchments (draining directly into the Adriatic Sea, to the right). For Adriatic catchments, k_{sn} is estimated both for the entire catchment (white symbols) and separately for the Apennine and the peri-Adriatic domains (colored symbols refer to the main lithologies outcropping in the analyzed catchments). (d–f) E versus k_{sn} plots with linear regressions to obtain an average K value for (d) the entire Adriatic catchments, (e) the Apennine belt, and (f) the peri-Adriatic belt. The linear regression (continuous red lines) uses a York fit forced through the origin (Racano et al., 2021, 2023; York et al., 2004) with standard error estimate (stippled red lines); corresponding K values are indicated in red above the plots. (g–i) Erodibility (K) values estimated individually for each catchment, for (g) the entire Adriatic catchments, (h) the Apennine belt, and (i) the peri-Adriatic belt. Panel (j) shows average K and k_{sn} values estimated for the main lithological classes; red and stippled lines show average K value for the Adriatic belt ($K_{b\text{mean}}$) and its standard error; $K_{p\text{mean}}$ is an inferred value for the peri-Adriatic belt.

Geochemistry, Geophysics, Geosystems

10.1029/2024GC011592

Table 2
Terrace and Paleosurface Ages, Strath Elevations, Incision Rates, and Dating Techniques for Bidente to Trigno Catchments

Catchment	Reference	Strath terrace/ Paleosurface level	Geological domain	Terrace strath/ Paleosurface elevation above thalweg (m)	Age (ka)	Incision rate (mm/yr)	Average incision rate (mm/yr)	Method
Bidente	Wegmann and Pazzaglia (2009)	Qt0	Apennine	388 ± 10	800 ± 100	0.5 ± 0.0004	1.3 ± 0.13	$^{26}Al/^{10}Be$ burial age
		Qt1		318 ± 10	620 ± 25	0.5 ± 0.0001		Relative MIS dating
		Qt2		196 ± 10	440 ± 25	0.4 ± 0.003		Relative MIS dating
		Qt3		123 ± 10	140 ± 10	0.9 ± 0.01		Relative MIS dating
		Qt4		48 ± 5	30 ± 5	1.6 ± 0.1		^{14}C dating
		Qt5		40 ± 5	22 ± 2	1.8 ± 0.1		^{14}C dating
		Qt6		27 ± 3	13 ± 2	2.1 ± 0.2		^{14}C dating
		Qt7		20 ± 2	9 ± 1	2.2 ± 0.1		^{14}C dating
		Qt8		6 ± 1	6 ± 1	1 ± 0.1		^{14}C dating
		Qt9		2.5 ± 0.5	1.5 ± 0.5	1.7 ± 0.4		^{14}C dating
Musone	Wegmann and Pazzaglia (2009)	IMO 2	peri-Adriatic	154 ± 5	775 ± 260	0.2 ± 0.004	0.55 ± 0.03	$^{26}Al/^{10}Be$ burial age
		Qt2		73 ± 15	450 ± 50	0.2 ± 0.002		Relative MIS dating
		Qt3		42 ± 22	160 ± 10	0.3 ± 0.02		$^{230}Th/^{234}U$ dating
		Qt4-5		25 ± 4	40 ± 5	0.6 ± 0.02		^{14}C dating
		Qt5		14 ± 1	27 ± 2	0.5 ± 0.003		^{14}C dating
		Qt7		11 ± 1	10 ± 1	1.1 ± 0.02		^{14}C dating
		Qt9		3 ± 0.5	3 ± 1	1 ± 0.1		Soil chronostratigraphy
Tesino	Delchiaro et al. (2024)	T1	peri-Adriatic	140 ± n/a	295.8 ± 131.7	0.365 ± 0.095	0.32 ± 0.05	OSL dating
		T2		90 ± n/a	133.1 ± 22.31	0.28 ± 0		OSL dating
		T3		45 ± n/a	26.3 ± 2.9	n/a ± n/a		OSL dating
Aterno-Pescara	Crescenti et al. (2015)	ACT	peri-Adriatic	150 ± 10	115 ± 10	1.3 ± 0.08	1.03 ± 0.07	Relative MIS, tephra and paleosoil dating
		AVM1		100 ± 10	85 ± 5	1.1 ± 0.06		Relative MIS, tephra and paleosoil dating
		AVM2		55 ± 5	77.5 ± 2.5	0.7 ± 0.07		Relative MIS, tephra and paleosoil dating
Alento	Crescenti et al. (2015)	ACT	peri-Adriatic	120 ± 10	115 ± 10	1.04 ± 0.13	0.85 ± 0.12	Relative MIS, tephra and paleosoil dating
		AVM1		85 ± 7	85 ± 5	1 ± 0.1		Relative MIS, tephra and paleosoil dating
		AVM2		40 ± 10	77.5 ± 2.5	0.51 ± 0.13		Relative MIS, tephra and paleosoil dating
Foro	Crescenti et al. (2015)	AVM1	peri-Adriatic	90 ± 10	85 ± 5	1.06 ± 0.13	0.88 ± 0.1	Relative MIS, tephra and paleosoil dating
		AVM2		55 ± 5	77.5 ± 2.5	0.7 ± 0.07		Relative MIS, tephra and paleosoil dating
Moro	Crescenti et al. (2015)	ACT	peri-Adriatic	140 ± 10	115 ± 10	1.21 ± 0.13	1.21 ± 0.13	Relative MIS, tephra and paleosoil dating
Trigno	Amato et al. (2017)	II	Apennine	500 ± 255	500 ± 90	1 ± 0.53	0.85 ± 0.47	$^{40}Ar/^{39}Ar$ tephra dating
		III		215 ± 75	311 ± 10	0.7 ± 0.41		$^{40}Ar/^{39}Ar$ tephra dating

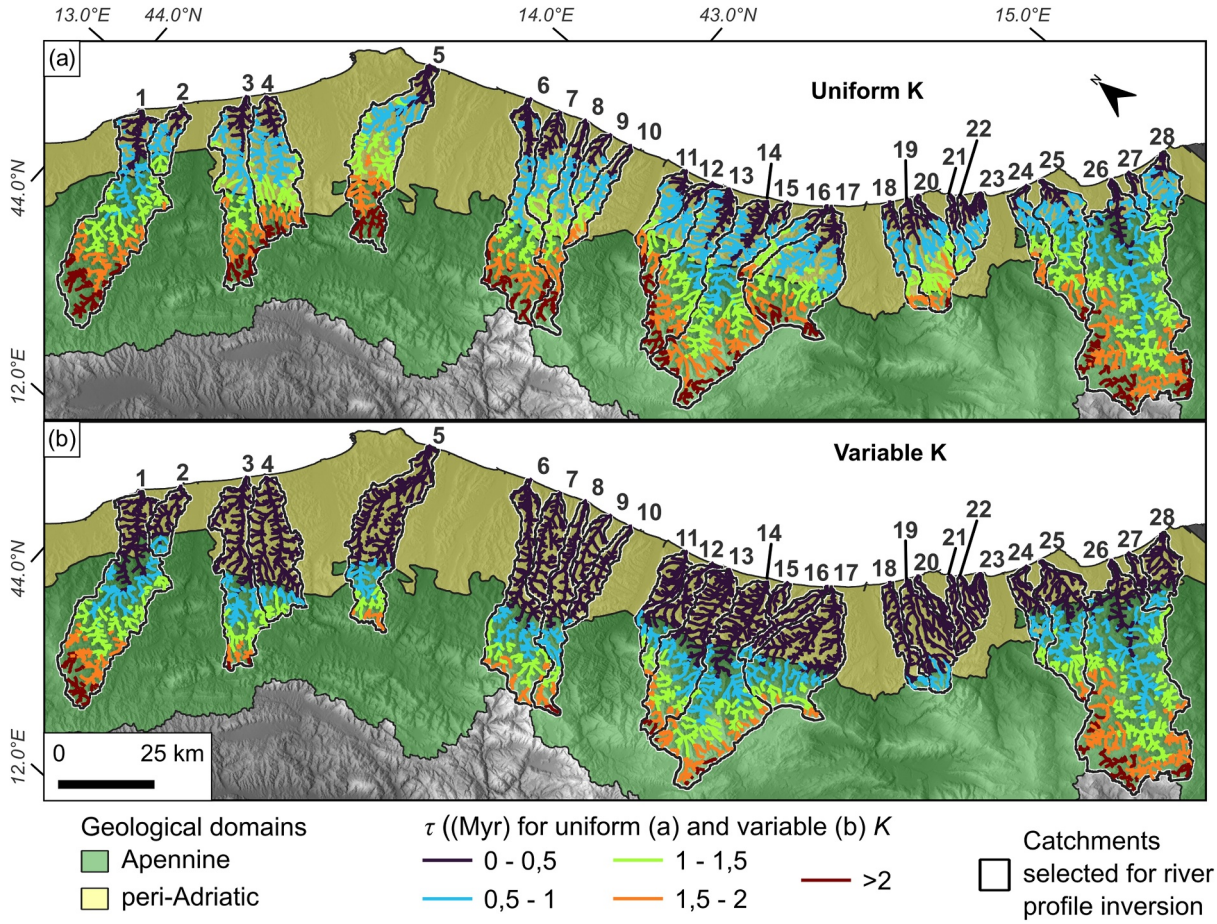

Figure 4. τ-maps of catchments selected for the linear river-profile inversion; (a) Using a single catchment-average value for K of 5.0×10^{-5} $m^{0.28}$/yr; (b) Using spatially variable K-values, differentiating between an average value for the Apennine domain (4.0×10^{-5} $m^{0.28}$/yr) and an average for the peri-Adriatic domain (1.5×10^{-4} $m^{0.28}$/yr).

The relationship between average k_{sn} and erosion rates (Figures 3d–3f) does not show a strong linear correlation, especially when including both the northern and Adriatic catchments (Figure 3d). The erodibility (K) inferred from the slope of the fit is $3.2 \pm 0.5 \times 10^{-5}$ $m^{0.28}$/yr, with a low R^2 (0.35). When including the northern catchments and only the Apennine part of the Adriatic catchments (Figure 3e), the R^2 value is higher (0.55), but the estimated K is almost the same ($3.1 \pm 0.5 \times 10^{-5}$ $m^{0.28}$/yr). Conversely, a linear fit of k_{sn} versus incision rates for the peri-Adriatic belt only (Figure 3f) shows a high R^2 value (0.84), and most of the points fall within the uncertainty boundaries of the linear fit. Scatter in this relationship may call into question the assumption of $n = 1$ (implied by a linear fit), although a non-linear function does not improve the fit. The resulting K value is an order of magnitude higher than the value for the Apennine belt at $1.5 \pm 0.5 \times 10^{-4}$ $m^{0.28}$/yr. These K values estimated by linear regressions are similar to K values estimated for the individual catchments (derived using Equation 13; Figure 3g), particularly when separating the Adriatic catchments into their Apennine and peri-Adriatic parts (Figures 3h and 3i).

For the Apennine belt, we derive a uniform erodibility value not only by estimating K for single catchments but also by estimating lithology-dependent K values obtained by dividing, in each catchment, the erosion rates by the average k_{sn} of the dominant bedrock lithologies (Figure 3j). The average k_{sn} varies somewhat between lithological classes, with mixed sedimentary rocks having the highest mean value and standard deviation. However, all values are consistent with an average K of $4.4 \pm 0.8 \times 10^{-5}$ $m^{0.28}$/yr, close to the average K estimated from single catchments. In the following, we apply either a constant K-value of 5.0×10^{-5} $m^{0.28}$/yr for the full catchments or a spatially variable K with a value of 4.0×10^{-5} $m^{0.28}$/yr for the Adriatic domain and 1.4×10^{-4} $m^{0.28}$/yr for the peri-Adriatic domain.

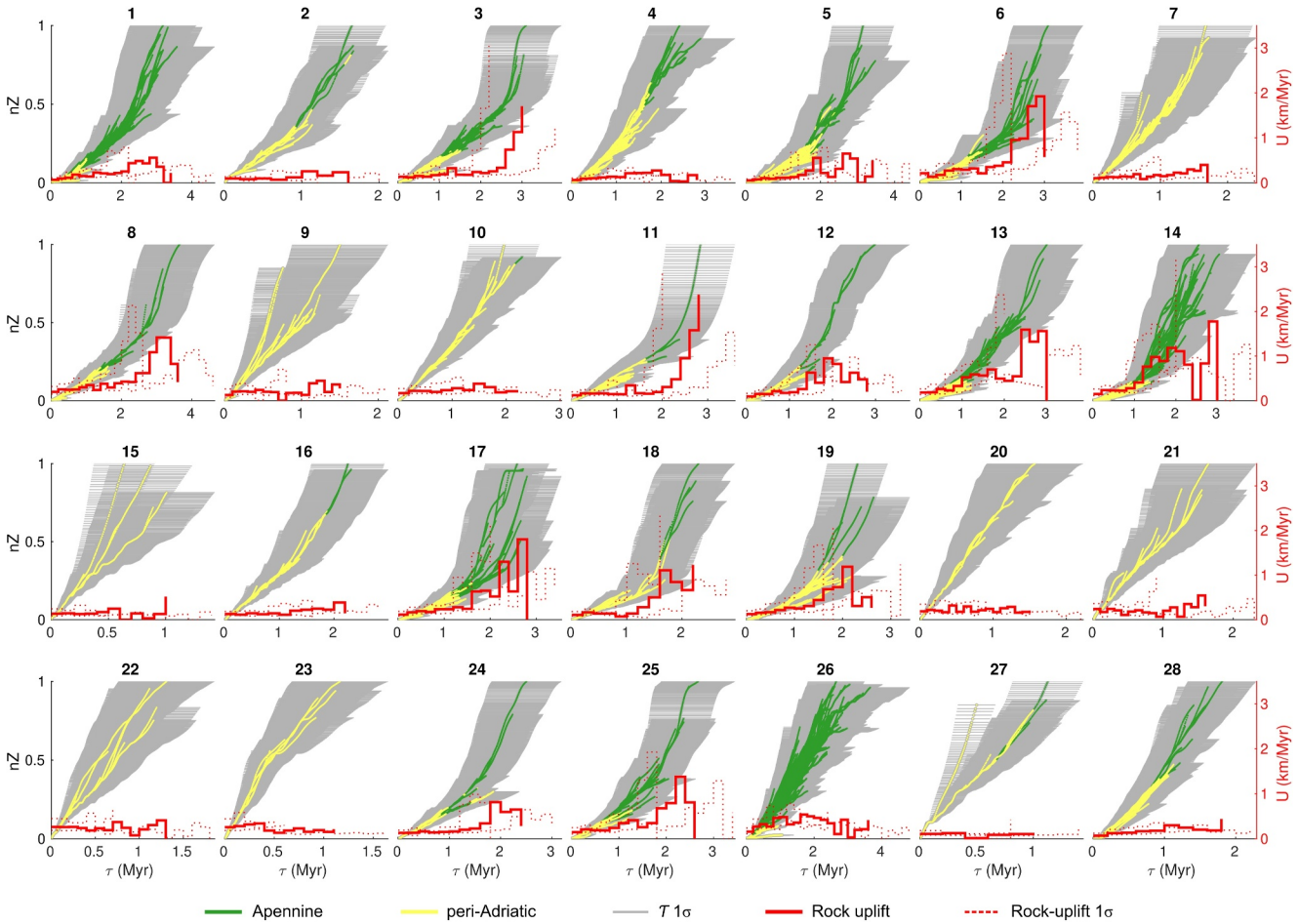

Figure 5. τ-plots for constant K of 5.0×10^{-5} $m^{0.28}$/yr, with normalized elevations, for the 28 catchments selected to reconstruct rock-uplift histories, and rock-uplift curves inferred from linear river-profile inversions. Green and yellow curves show river profiles in the Apennine and peri-Adriatic domains, respectively; gray shading shows 1σ uncertainty on τ-values; continuous and dotted red curves show inferred uplift rates and their uncertainty through time. Note variable τ-scale for each plot.

4.2. Timing of River Incision and Spatiotemporal Patterns of Rock Uplift

The estimation of τ in the 28 catchments selected for river-profile inversions yields different response times, depending on the use of uniform versus variable K. Generally, the maximum response times for catchments that drain the Apennine domain are quite consistent across different τ estimations, up to ca 3 Myr (Figure 4). Differences become evident when focusing separately on the Apennine and peri-Adriatic domains. Assuming a uniform K across the study area, τ lies between 1 and 2 Myr at the boundary between the Apennine and peri-Adriatic domains (Figure 4a), whereas assuming different K values for the Apennine and peri-Adriatic domains (Figure 4b) leads to an average τ at the boundary between the two domains of around 0.5 Myr.

Similar to the τ estimates, inferred rock-uplift histories also exhibit differences depending on the chosen approach. For uniform K (Figure 5), most of the rock-uplift histories going back to at least 3 Ma show a peak in rock-uplift rate between 3 and 2 Ma, with maximum rates reaching approximately 2 km/Myr. From 2 Ma onward, inferred rock-uplift rates rapidly decrease, reaching a near steady-state trend and not exceeding 0.5 km/Myr until the present. Catchment 26 shows a different rock-uplift trend, with rates increasing and decreasing more progressively than for the other catchments, reaching a peak of 0.6 km/Myr around 1.7 Ma. The rock-uplift histories inferred by assuming variable K (Figure 6) show significantly different rates and trends. The highest uplift rates are reached early on in the inversions, similar to the uniform K histories, but these maximum rates are higher, surpassing 2 km/Myr. The timing of the peak in uplift rates is also generally younger than that recorded for constant K, ranging between 2.5 and 1.5 Ma, after which uplift rates progressively decrease. The largest differences between inferred rock-uplift histories using the two approaches are evident for the Middle Pleistocene to

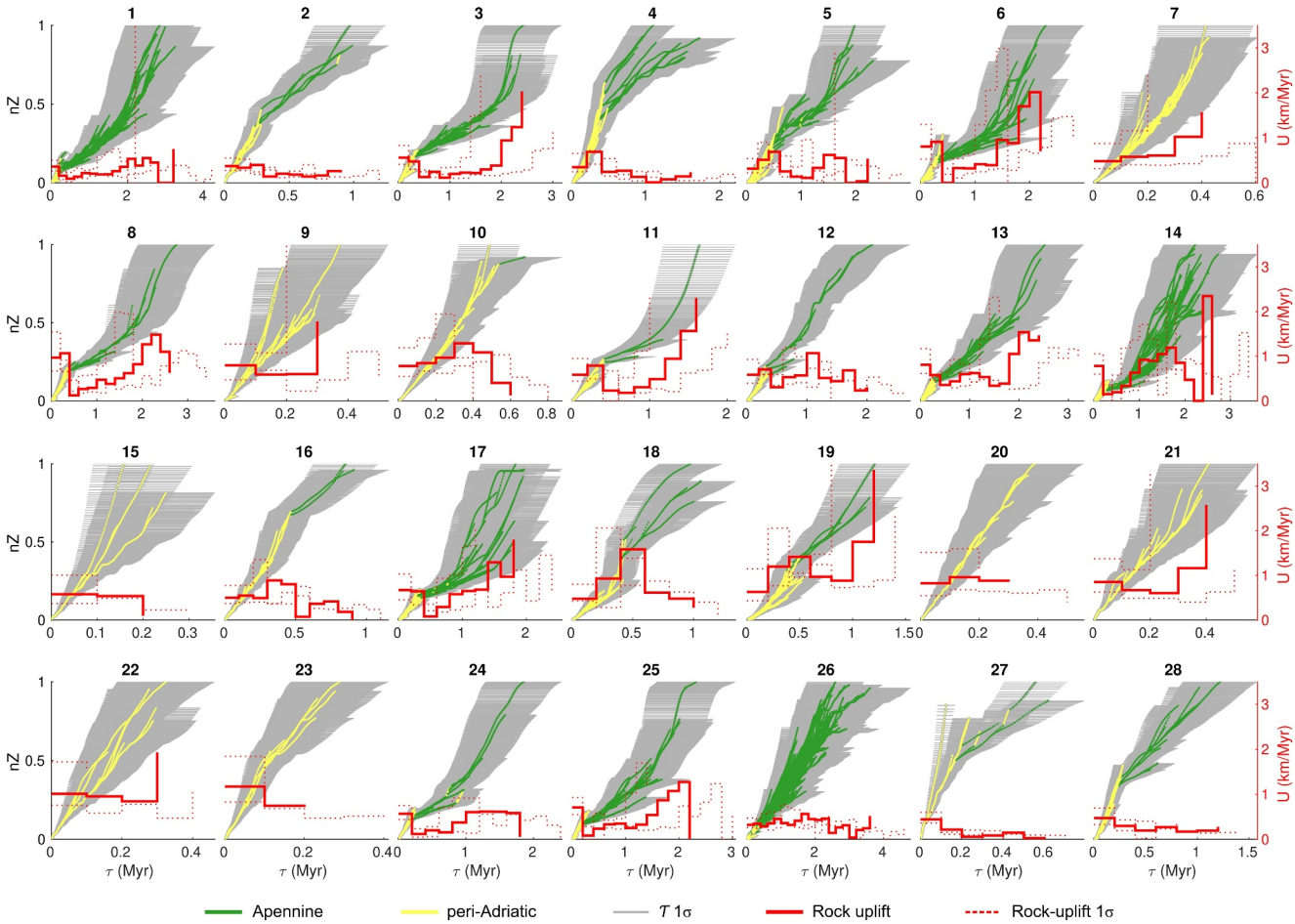

Figure 6. As Figure 5 but for spatially variable K, with different values for the Apennine (4.0×10^{-5} $m^{0.28}$/yr) and peri-Adriatic (1.5×10^{-4} $m^{0.28}$/yr) domains.

Holocene rates. In reconstructions assuming variable K, rock-uplift rates in most catchments start to increase again from 0.5 to 0.7 Ma, reaching rates up to 1 km/Myr for some catchments.

4.3. Impact of Coastal Lengthening on River Profile Inversions From LEM Simulations

In order to assess the robustness of our inferred rock-uplift histories in the face of the seaward lengthening of catchments discussed previously as well as to assess the effects of including constant versus spatially variable rock erodibility in the inversions, we ran a series of LEM simulations including different coastal-uplift scenarios (see Section 3.4 for details) and inverted the predicted present-day river profiles using the same procedure as above. The input rock-uplift history in these LEM simulations was modeled on the general outcome of the inversions discussed above: each simulation runs for a total time of 5 Myr and is divided into 4 stages with different uplift rates: (a) 0.5 km/Myr in the first 2 Myr (5–3 Ma), (b) 2 km/Myr from 2 to 4 Myr (3–1 Ma), (c) 0.5 km/Myr from 4 to 4.75 Myr (1–0.25 Ma), and (d) 1 km/Myr from 4.75 to 5 Myr (0.25 Ma to present) (Figure 7a). The models include spatially variable erodibility modeled on the average inferred K values for the Apennine and peri-Adriatic sectors of the studied catchments (Figure 7b).

For the control (uniform uplift) model and sudden coastal uplift (sudden catchment lengthening) LEM simulations, the final main catchments show similar stream networks and comparable drainage areas (Figures 7c and 7e), while for the progressive coastal uplift (progressive catchment lengthening) simulation, the main catchment has a smaller drainage area and becomes narrower as it extends coastward (Figure 7d). In general, the three simulations record an incision history covering the final 2.5–2.75 Myr of the simulations, inferred by calculating τ on the main drainage system.

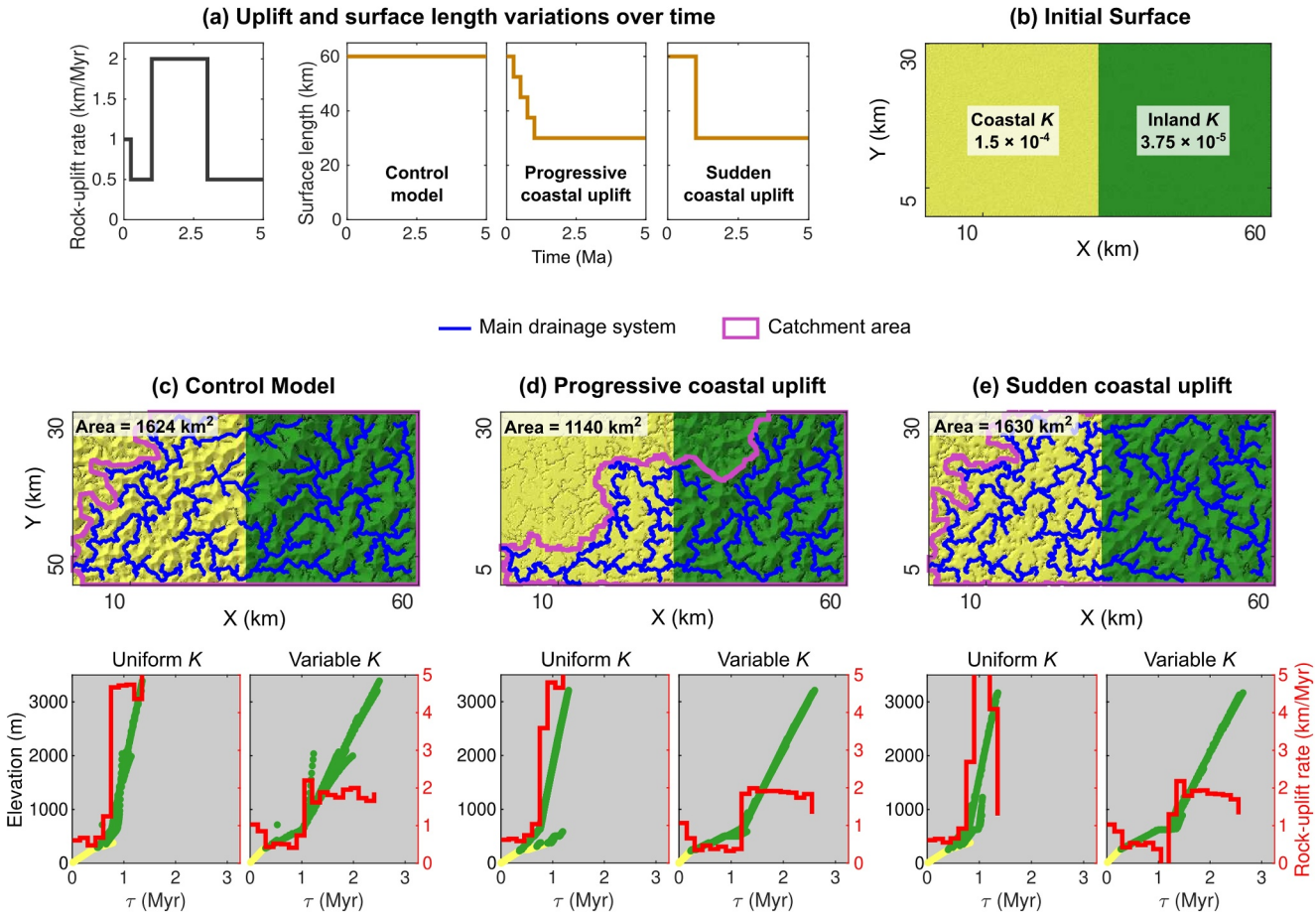

Figure 7. (a) Rock-uplift rates and surface length variations imposed in the landscape-evolution model (TTLEM) simulations, (b) initial surface used to run the three simulations, colored by imposed *K*-value, and final stream network of the main drainage system from (c) the Control model, (d) the Progressive coastal uplift model, and (e) the Sudden coastal uplift model. Outline of the largest catchment used for river-profile inversion is shown in purple; drainage area for this catchment is indicated at the top left. Lower panels show river profiles for the largest catchment in τ-space, colored by imposed *K*-value, and results of linear inversions (red lines) using both constant (left panels) and variable (right panels) *K* for these profiles.

The rock-uplift histories inferred from inversions of final river profiles predicted by these three simulations are not significantly different. The rock-uplift history inferred from the progressive coastal uplift model (Figure 7d) shows the closest match between the imposed and reconstructed rock-uplift histories in terms of both the rock-uplift rates and the timing of changes. The river-profile inversion of the control model exhibits noise produced by drainage capture events (Figure 7c and Movie S1), while inversions derived from the simulation including sudden coastal uplift exaggerate the minimum and maximum uplift-rate peaks at τ between 1.0 and 1.5 Myr (Figure 7e). For all three simulations, however, there are significant differences between the rock-uplift histories assuming spatially uniform versus variable *K*.

For the inversions assuming uniform *K*, the τ-plots of each simulation show two different zones that, even when the catchments reach steady-state conditions, have different slopes (e.g., Movie S1 at $t = 4.75$ Myr), indicating a static slope-break zone between the inland belt (higher steepness, lower *K*) and the coastal belt (lower steepness, higher *K*). The uplift histories derived from uniform-*K* models exhibit trends that contrast with the uplift variations imposed in the models, in which uplift rates are mostly overestimated and the final increase in uplift rate at 0.25 Ma is not captured (Figure 7, Movies S1–S3).

In contrast, for the inversions assuming variable *K*, the τ-plots do not exhibit a constant slope-break at the boundary between the inland and coastal belts, and slope changes in the τ-plot consistently coincide with imposed changes in uplift rates (Figures 7c–7e, Movies S1–S3). As a result, the rock-uplift histories inferred by inverting

the K-variable τ-plots generally reflect well the imposed uplift variations (Figures 7c–7e, Movies S1–S3). The τ-plots also appear to be less scattered than those obtained for the inversions assuming uniform K.

4.4. Spatio-Temporal Patterns of Rock Uplift

Combining the inversion results for individual catchments allows visualizing spatio-temporal patterns of rock uplift (Figure 8), which highlight differences in inferred rock-uplift histories depending on the assumptions about K. When assuming a uniform K-value throughout the catchments, the spatio-temporal rock-uplift model (Figure 8c) indicates a phase of accelerated rock uplift between 3.0 and 2.5 Ma, with rates of up to 1.5 km/Myr occurring between the Sibillini and Gran Sasso ranges (Figures 8a and 8b). West of the Maiella Massif, the rock-uplift acceleration model (i.e., the time derivative of rock uplift rates; Figure 8d) shows a wave of accelerating rock uplift that migrates southward at a rate of ∼60 km/Myr from ca. 2.7 to 2.0 Ma. This migration remains evident when changing the smoothing degree of the interpolated data (Figure S11 in Supporting Information S1). From 2.0 to 1.5 Ma, the rock-uplift rate decelerates significantly, and subsequently slows down further until reaching a rate of approximately 0.2 km/Myr in the last 0.5 Myr (Figures 8c and 8d).

When assuming variable K (Figures 8e and 8f), a phase of rapid rock uplift occurs between approximately 3.0 and 1.5 Ma, with a peak in uplift rates recorded around 2.5 Ma between the Laga Massif and Gran Sasso range (Figure 8). Starting from the Gran Sasso area, a wave of rapid rock-uplift propagates southward at a rate of ∼90 km/Myr, with maximum acceleration in rock-uplift rate occurring between 2.7 and 1.5 Ma (Figure 8f), progressively decreasing in magnitude. As for the constant-K model, this trend is robust when changing the degree of smoothing in the interpolation (Figure S12 in Supporting Information S1). The model of rock-uplift acceleration also indicates a rapid deceleration in the rock-uplift rate after 2.5 Ma, particularly between the Sibillini and Gran Sasso ranges. In contrast to the results assuming uniform K, however, rock-uplift rates accelerate again after 1 Ma. The onset of this second accelerated uplift phase, with maximum rates between 0.8 and 1 km/Myr, does not show a clear spatial migration pattern but rather seems to be coeval across the entire study area. At the latitude of the Maiella Massif, rock-uplift rates remain high, at ca 0.8 km/Myr over the last 1 Myr (Figure 8e). In the northwestern half of the study area (catchments 1 to 13), rock-uplift acceleration started earlier (around 1.2 Ma), while in the southern catchments, rock-uplift rates started accelerating around 0.5 Ma and continued to accelerate to the present (Figure 8f).

5. Discussion

5.1. Estimation of the Erodibility Coefficient (K) From Coastal Incision Rates

The main challenge for inverting the Adriatic river profiles to reconstruct the rock-uplift history of the region lies in accurately estimating the erodibility coefficient (K) for the rocks of the Apennine domain. Considering that the denudation rates are derived from *in situ* produced ^{10}Be in quartz (von Blanckenburg, 2005), we have no direct constraints on denudation rates of non-quartz-bearing rock units, including the pelagic and carbonate-platform limestones that dominate the central Apennines. Moreover, for the Adriatic catchments, most of the incision rates from dated paleosurfaces and fluvial terraces are limited to the peri-Adriatic domain. The only incision rates that include the Apennine belt are primarily derived from siliciclastic turbiditic units, based on the incision rates of strath terraces in the Bidente catchment and on modeling knickpoint migration on the Tronto River, which was calibrated with dated travertines (Sembroni et al., 2020; Tables 1 and 2). Despite having similar bedrock compositions, these catchments provide different incision rates: approximately 1.3 km/Myr for the Bidente and around 0.6 km/Myr for the Tronto. The incision rate from the Trigno catchment is also representative of the Apennine domain, including a broader range of lithologies such as mixed carbonate and siliciclastic turbidites, and Cretaceous to Miocene clays (Figure 2a). The average incision rate (∼0.8 km/Myr) is close to that of the Tronto catchment; however, it does not provide direct estimates of incision rates of the Apennine limestones.

Despite these limitations, modern denudation rates in the northern catchments (those draining to the Po Plain foreland; Figure 2) and estimated K values (Figures 3h and 3j) do not show a significant dependency on the main outcropping lithologies. Also, modern denudation rates throughout the study area (0.19–0.65 km/Myr) as well as paleo-denudation rates inferred from lower Pleistocene shallow marine deposits between the Esino and Reno catchments (∼0.3 km/Myr; Cyr & Granger, 2008) are similar to most terrace incision rates (∼0.5 km/Myr), even though the latter tend to increase for younger terraces (Figure 9; see discussion in the following section). Moreover, variations in peri-Adriatic incision rates (white diamonds in Figure 3a) appear to track variations in

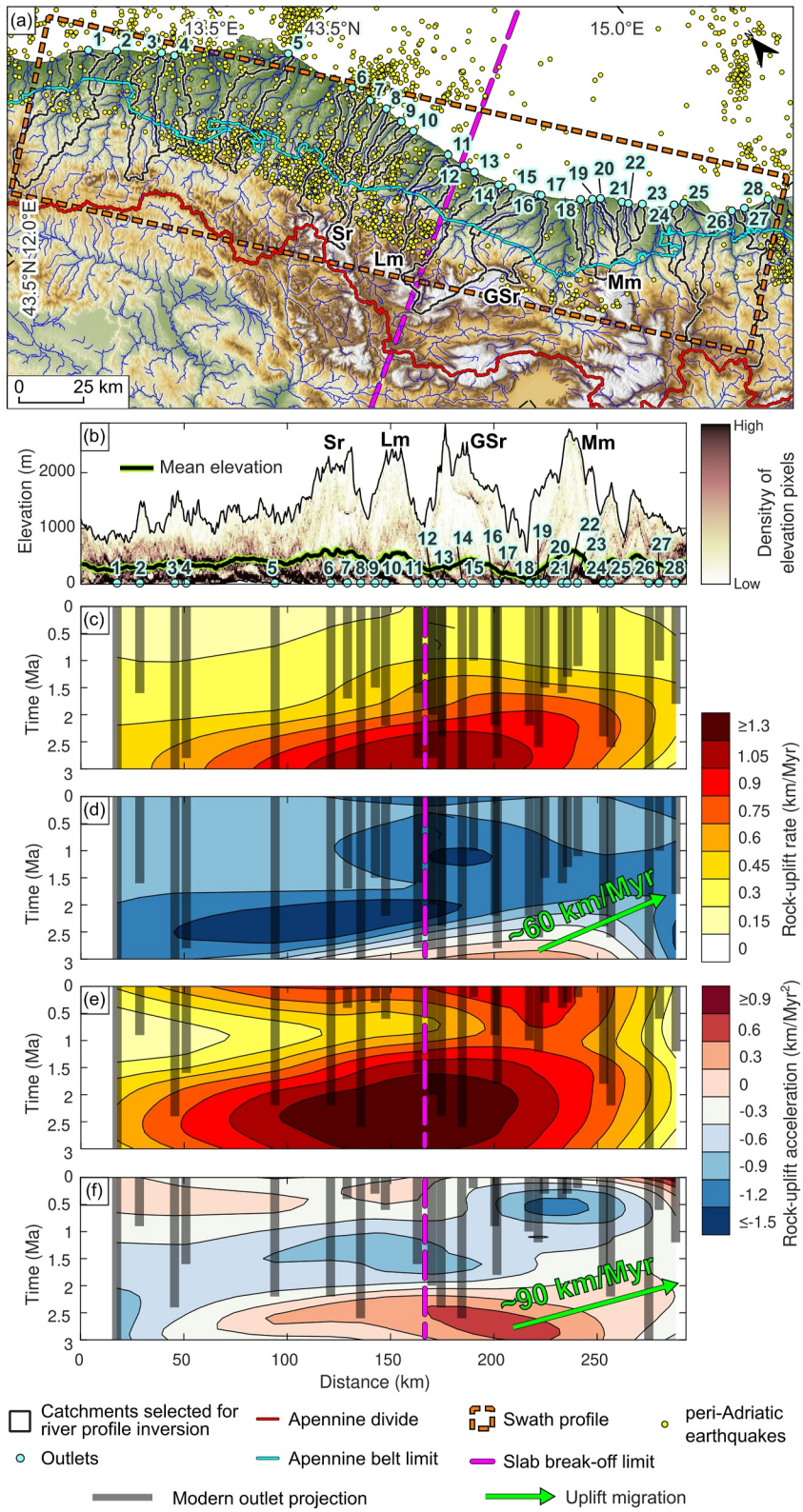

Figure 8.

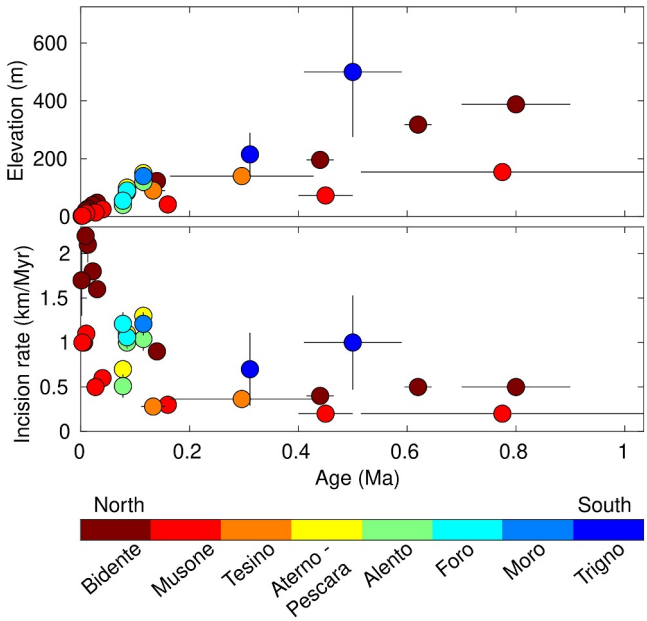

Figure 9. Plots of age versus elevation and age versus incision rate for the dated paleosurfaces and fluvial terraces along rivers draining to the Po Plain (Bidente catchment) and the Adriatic Sea (Musone to Trigno catchments).

average k_{sn} of the Adriatic catchments, especially when considering the Apennine domain only (Figure 3c). For example, between the Esino and Trigno catchments, both incision rates (Figure 3a) and k_{sn} (Figure 3c) tend to increase to the south, suggesting a direct correlation between river incision rates (measured in the peri-Adriatic domain) and river steepness (in the Apennine domain) for these catchments. Similarly, on Crete, Ott et al. (2019) found comparable erosion rates between carbonate and clastic lithologies, but due to higher infiltration rates, steepness values were generally higher in the carbonates. Following these arguments, we consider the peri-Adriatic incision rates as an acceptable proxy for the catchment-average incision rates, supporting their use to estimate K for both the Apennine and peri-Adriatic domains.

A good correlation also exists between incision rates and average k_{sn} of the peri-Adriatic belt, as evidenced by the relatively high R^2 value of their linear fit (Figure 3f). The K values estimated for individual catchments tend to converge toward an average value (Figures 3g–3i), which is consistent with the K values inferred from linear regression of erosion/incision rates versus average steepness index (Figures 3d–3f), providing confidence in the K values used in the river-profile inversions. As noted earlier, scatter in the linear fit may cast doubt on our assumption of $n = 1$. Without additional constraints, we cannot justify a different assumed value, but we acknowledge that the timescale of our inversion results would change if n were not equal to 1.

5.2. Reliability of the Reconstructed Rock-Uplift Histories and Independent Geochronological Constraints

Our LEM simulations show that downstream lengthening of river channels, even when comprising a substantial proportion of the catchment, has little to no effect on τ-plots, and consequently has little to no effect on rock-uplift histories reconstructed from river-profile inversions, at least in the scenarios we explored. The reason for this limited effect lies in the definition of χ (and therefore τ; Equations 5 and 9): because χ scales with the inverse of drainage area integrated from downstream to upstream, adding drainage area at the downstream end of a catchment through lengthening has a much smaller effect on χ than adding drainage area at the upstream end, such as through drainage capture.

The rock-uplift history derived from river-profile inversion that best reflects imposed rock-uplift variations is the one reconstructed from the progressive coastal uplift model and assuming different K values for the Apennine and peri-Adriatic domains for the inversions (Figure 7d, Movie S2). Inversions that assume uniform K yield poor results for all three simulations (Figure 7); this is to be expected, since the forward models used to predict the inverted river profiles included different K values for the Apennine and peri-Adriatic domains.

Rock-uplift histories reconstructed from the uniform uplift and sudden coastal uplift models both exhibit some changes in rock-uplift rates unrelated to the imposed variations. The uniform-uplift scenario shows a rock-uplift peak higher than 2 km/Myr at the moment when the imposed rock-uplift rates decrease from 2 to 0.5 km/Myr. This behavior appears to relate to a river channel in the τ-plot that is influenced by the effect of upstream area capture (Figure 4c, Movie S1). The sudden coastal uplift model displays a rapid jump and drop from rates higher than 2 km/Myr to 0 km/Myr at τ between 1 and 1.7 Myr (Figure 4e; Movie S3). This perturbation represents the effect of the sudden uplift of the 30-km wide coastal belt, which produces an upstream propagating flat zone, for

Figure 8. (a) Instrumental seismicity recorded in the peri-Adriatic belt, and location of the highest massifs and ranges of the Adriatic flank of the Apennines: Sr: Sibillini Range (max. 2,476 m a.s.l); Lm: Laga Massif (max. 2,458 m a.s.l.); GSr: Gran Sasso Range (max. 2,912 m a.s.l.); Mm: Maiella Massif (max. 2,793 m a.s.l.). The purple line traces the limit between seismic and near-aseismic regions, marking the northern boundary of possible slab break-off; the orange-dashed box outlines the swath profile shown in b. (b) Topographic swath profile showing mean and maximum elevations and colored as a heatmap following the density of the points at a given elevation, and location of the outlets of the catchments used for river-profile inversion; (c) Spatiotemporal rock-uplift model for constant K; gray bars indicate constraints from individual river-profile inversions, purple line is as in (a); (d) Spatiotemporal rock-uplift acceleration model (i.e., temporal derivative of rock-uplift rate) for constant K; green arrow indicates estimated propagation velocity of the uplift pulse. Panels (e, f) as (c) and (d) but for spatially variable K.

which the slope in the τ-plot is not linked to a drop in uplift rate but rather to the geometry of the uplifted downstream surface. Apart from this artifact, the uplift history is generally well reproduced. Considering that the progressive coastal uplift with progressive channel lengthening model is closest to the history we envision for the study region, we are confident that our river-profile inversions, particularly those that assume different K values for the Apennine versus the peri-Adriatic domains, provide a robust reconstruction of past rock-uplift rates.

The TTLEM simulations, in particular the sudden coastal uplift model, provide another important insight concerning the fluvial response time τ versus the age (of emergence) of the topography. The parts of the landscape for which τ is larger than the age at which the topography emerged will not provide an accurate inverted uplift history, as demonstrated by the sudden coastal uplift model. However, the largest catchments that we studied correspond to maximum response times of ∼3 Myr (Figures 4 and 6), whereas sedimentological, paleontological and morphostratigraphic data indicate that most of the Apennine chain was emerged before 3 Ma (e.g., Cosentino et al., 2010, 2017; Galadini et al., 2003, and references therein). Formation of a drainage network at that time is also demonstrated by the presence, in some intra-Apennine basins, of continental sediments older than 3 Ma (e.g., Bosi et al., 2003; Cosentino et al., 2017; Pandeli et al., 2009). We therefore infer that our inverted rock-uplift histories, even for their oldest parts, are robust.

Finally, our inversion results depend on the assumption that the erodibility coefficient, K, is constant through time. K tends to vary spatially mostly as a function of lithology, but temporal changes in climate may also influence it. Over the timescale of our inversions (i.e., several million years), and the temporal resolution of the modeling (200 kyr), we do not expect any resolvable impact from climate changes on K related to orbital timescales. However, there could be some resolvable impact considering the growth of topography through time, if that topography influenced rainfall patterns in the catchments of interest. There is no strong asymmetry in modern precipitation across the Apennine chain at the latitude of our study site (Figure S1 in Supporting Information S1). Growing topography may, nevertheless, "capture" more precipitation, and thus increase the erodibility through time. If true, this would mean that rock-uplift rates (derived from U/K) in the latter stages of our inversion would be underestimated or that rock-uplift rates in the early stages of our inversion would be overestimated. The latter is more likely given that we calibrate K based on geologic constraints on rock uplift that average over late Pleistocene to Holocene timescales or based on present-day geodetic measurements. But even a reduction in the early uplift rates by ca. 50% would not have a substantial impact on the results we present. Also, importantly, any topographically induced change in precipitation is likely to occur gradually over time, and thus its impacts on the spatio-temporal pattern of rock-uplift that we infer, which shows both increases and decreases in rock-uplift spatially and temporally, are unlikely to change that pattern in a way that would alter our conclusions. Temporal changes in K would also make the response time τ variable over time, thus modifying the timing of inferred changes in uplift rates. However, as discussed below, the uplift history reconstructed from the river-profile inversions is supported by other geological constraints, allowing us to assert that the gradient variations recorded in the rivers can be predominantly attributed to changes in uplift over time.

Several studies have suggested that the Northern and Central Apennines experienced a phase of accelerated rock uplift around 2.5 Ma (Cosentino et al., 2017; Fellin et al., 2021; Pazzaglia & Fisher, 2022; San Jose et al., 2020). Our results corroborate this inference and provide novel temporal and spatial constraints for this accelerated uplift phase. Our inversions suggest that the most rapid rock-uplift rates during this phase coincide spatially with the highest elevations of the Apennine belt (Figure 8). The modeled rock-uplift trends suggest that the accelerated rock-uplift phase was not coeval along the entire Apennine belt; it initially affected the northern-central belt up to the Gran Sasso Range, and then migrated southward over time at a rate of ca. 90 km/Myr in our preferred model (Figure 8f).

The timing of the rock-uplift rate acceleration inferred from the models corresponds to the onset of uplift and normal faulting in the inner Apennine chain, as the development of the Apennine intra-montane basins started after 3 Ma (Cosentino et al., 2017). Also, thermochronology (Fellin et al., 2021) and oxygen-isotope (San Jose et al., 2020) data indicate the onset of accelerated exhumation and surface uplift at around 2.5 Ma. The constant-K uplift model (Figure 8c) suggests that maximum uplift rates occurred around 3 Ma and then started decreasing, whereas the variable-K model (Figure 8e) records the onset of the accelerated uplift phase from ca. 3 Ma and maximum rock-uplift rates between 2.5 and 2 Ma. The latter results align better with the independent chronological constraints, providing further support for the notion that the variable-K approach provides a more accurate reconstruction of the Apennine rock-uplift history.

Furthermore, the rock-uplift model generated with variable K (Figure 5e) provides new insights into the rock-uplift history of the Maiella Massif, which has been a topic of debate. The presence of foredeep deposits overthrust by the Maiella anticline suggests an initiation of compression during the Early Pliocene (Centamore & Rossi, 2009; Cosentino et al., 2010), while the uplift of littoral conglomerates along its eastern margin, dated to the Middle Pleistocene (Pizzi, 2003), suggests that the Maiella Massif was involved in the Middle Pleistocene uplift phase that affected the peri-Adriatic belt. In our variable-K model, the Maiella Massif experienced the most rapid rock uplift at ∼2 Ma (Figures 8e and 8f). Unlike other parts of the study area, rock-uplift rates in the Maiella area never dropped below 0.75 km/Myr. These results suggest that, in this specific area, rapid uplift persisted over time, continuing to uplift the Maiella Massif during the Middle Pleistocene (Pizzi, 2003).

Our reconstructed rock-uplift history also provides new insights regarding the uplift of the peri-Adriatic belt. Cosmogenic burial ages of the most recent marine deposits in the northern peri-Adriatic belt suggest that shallow-water marine deposition was still ongoing at around 0.9 Ma (Cyr & Granger, 2008), while pollen, fossil, and paleomagnetic analysis of the upper conglomeratic units in the southern part of the belt indicate ongoing coastal deposition at around 0.7 Ma (Pieruccini et al., 2016). The variable-K uplift model (Figure 8e) shows an acceleration in rock-uplift rates after this time, with rates rapidly increasing from 0.4 to 0.9 km/Myr between the Middle Pleistocene and the present. This result appears to contrast with the near-constant Pleistocene denudation rates inferred by Cyr and Granger (2008), a scenario that fits better with the constant-K uplift model, which predicts constant rock-uplift rates since the Early Pleistocene (Figure 8c). However, paleosurface and terrace incision rates also suggest a significant acceleration of incision after 0.3 Ma (Figure 9), with rates reaching up to 2 km/Myr for the Late Pleistocene/Holocene (Table 2). It has been argued that apparent increases in incision rates with shorter measurement intervals are a widespread phenomenon that reflects episodic hiatuses in river incision, or non-stationarity in the river-bed elevation, rather than a real increase in incision rates through time (Finnegan et al., 2014; Gallen et al., 2015). While the recent increase in incision rates apparent from the peri-Adriatic data (Figure 9) could potentially also be explained by such a bias, the consistency with the geological record discussed above, as well as with the predictions of the preferred variable-K uplift model, suggest it may be real. Additionally, present-day vertical velocities measured by GNSS suggest that most of the Central Apennines and of the peri-Adriatic belt are currently uplifting at rates of up to 1 km/Myr (Faccenna et al., 2014; Serpelloni et al., 2013).

Our results contrast with those obtained by Pazzaglia and Fisher (2022), who also reconstructed the Quaternary uplift history of the Apennines using linear inversions of river profiles. The main differences with our approach are that Pazzaglia and Fisher (2022) used a different ratio of m/n (they used the "standard" value of 0.45, whereas we estimated m/n directly from the fluvial drainage network) and a variable K estimated independently for all the main lithologies exposed in the inverted drainage basins. Although Pazzaglia and Fisher (2022) also infer an acceleration of uplift after 3 Ma in the northern and central Apennines, the rates of uplift they infer are significantly slower than those calculated here (∼0.25 km/Myr vs. ∼1 km/Myr at 2.5 Ma), and they do not record a second increment of rock uplift in the last 1 Myr. These differences may be attributed to the approach used to estimate K and to the use of an m/n value that is not directly representative of the Apennine belt. Indeed, k_{sn} and χ, and consequently τ and rock uplift, are very sensitive to the chosen ratio of m/n (Gailleton et al., 2021), and can vary by different orders of magnitude. Therefore, estimating an m/n ratio that is representative of the river profiles used for inversions is essential to obtain the most accurate results (Goren et al., 2014).

5.3. Topographic Evolution of the Central Apennines and Driving Mechanisms for Rock-Uplift

The present Apennine topography is the result of different tectonic regimes that have succeeded each other from the Miocene to the Quaternary (Cosentino et al., 2010). Several authors have proposed a model of topographic evolution divided into two main stages: a first stage driven by compression, which produced low topographic ridges that are represented today by a high-elevation relict landscape in the Apennines (Cosentino et al., 2010; Galadini et al., 2003), and a second stage linked to regional uplift and normal faulting, which is responsible for the present-day high-relief topography (Cosentino et al., 2017; Fellin et al., 2021; Galadini et al., 2003; San Jose et al., 2020).

Figure 10a shows a model of the topography that existed before the Quaternary uplift pulse, obtained by subtracting the cumulative uplift from river-profile inversions from the maximum current topography of the eastern Apennine range. Cumulative post-3 Ma rock uplift is highest in the central Apennines, consistent with the present-day topographic high in the same area (D'Agostino et al., 2001; Lanari et al., 2023; Molin & Fubelli, 2005; San

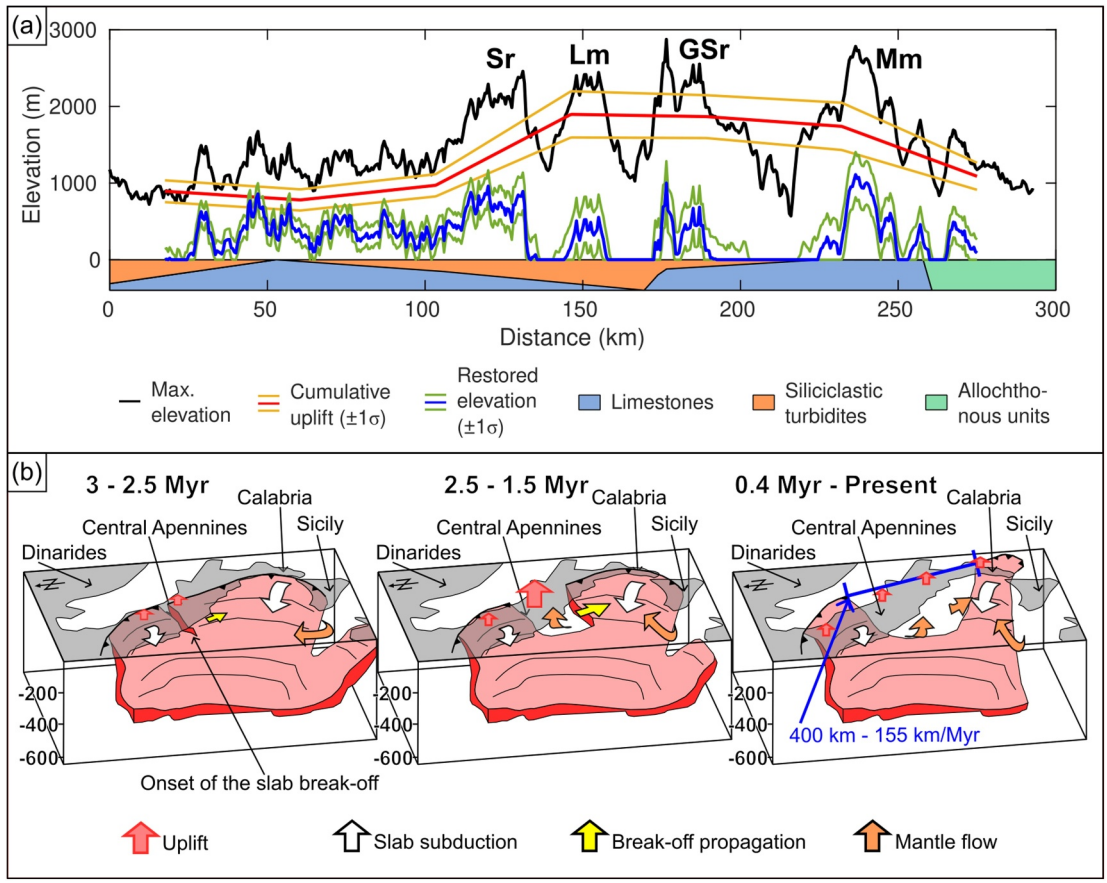

Figure 10. (a) Maximum elevation (black) of the swath profile in Figure 8 and location of the highest mountainous massifs (abbreviations as in Figure 8), cumulative uplift inferred from the uplift models calculated for variable *K*, and restored pre-Quaternary topography. The colored band at the bottom of the plot indicates the spatial variability of the main lithologies making up the Adriatic flank of the Apennines; (b) Cartoons illustrating the three-stage evolution of the Apennine range during the last 3 Myr, following slab tearing and southward migration of slab break-off.

Jose et al., 2020). This concurrence suggests that during the Quaternary, the currently highest Apennine massifs (Sibillini and Gran Sasso Ranges, Laga and Maiella Massifs) gained more elevation (approximately 1,300–2,000 m) than the ranges to their north and south (approximately 900–1,100 m). Such high cumulative uplift in the central Apennines is also demonstrated by a few outcrops of marine clays and sands dated to the Early Pliocene (biozone MNN16a), currently located at elevations of up to 2,000 m (*Argille e Sabbie di Pagliare* formation, Centamore, Crescenti, Dramis, Bigi, et al., 2006; Centamore, Crescenti, Dramis, Boncio, et al., 2006). The restored elevations of the central Apennines (Figure 6a) suggest that the topography before the Quaternary rock-uplift pulse was relatively constant along the Adriatic flank of the range, independent of the main lithologies characterizing the different sectors. The restored elevations lie at similar elevations and do not exceed 1,000 m, supporting the idea of a relatively low-relief landscape before the Quaternary (Galadini et al., 2003).

The spatiotemporal rock-uplift variations inferred from linear inversions of river profiles can provide new insights into the mechanisms driving regional rock uplift (e.g., Clementucci et al., 2023; McNab et al., 2018; Molin et al., 2023; Pan et al., 2023; Racano et al., 2021, 2023). In particular, our new rock-uplift model for the Apennine chain, characterized by a southeast-ward migrating pulse of rapid rock uplift, is consistent with uplift driven by southeast-ward migrating break-off of the Adria slab during the Quaternary (Faccenna et al., 2014). Numerical models suggest that a rapid but short-lived phase of accelerated uplift, resulting in topographic growth, is a signature of slab break-off, with the magnitude and duration of uplift depending on the depth of break-off (Duretz & Gerya, 2013; Magni et al., 2017). Field studies have corroborated these findings, for instance at the southern margin of the Central Anatolian Plateau, where the rock-uplift history inferred from river profiles was used to track the temporal propagation of slab break-off (Racano et al., 2021). Along the Apennine chain, the main

processes invoked to explain Quaternary uplift and the related onset of normal faulting are back-arc extension driven by slab roll-back and/or slab break-off and mantle upwelling (Cavinato & De Celles, 1999; Cosentino et al., 2017; D'Agostino et al., 2001, 2011; Faccenna et al., 2014; Fellin et al., 2021; San Jose et al., 2020). While current seismicity suggests that subduction is still active in the northern Apennines, several observations support the absence of a slab under the central part of the belt. They include: (a) the occurrence of a shallow slab gap inferred from seismic tomography (Faccenna et al., 2004, 2014; Giacomuzzi et al., 2012; Piromallo & Morelli, 2003; Wortel & Spakman, 2000); (b) the lack of deep seismicity (>30 km) (Chiarabba et al., 2005; Serpelloni et al., 2013); (c) the absence of active compressional deformation (Casero, 2004; Chiarabba et al., 2005, 2010, 2014; Faccenna et al., 2014); (d) the absence of earthquakes with compressional focal mechanisms (Montone et al., 1999, 2004, 2012); and (e) the progressive closure and uplift of the Bradanic Trough, the youngest foredeep basin of the southern Apennines, between the Middle and the Late Pleistocene (Tropeano et al., 2002).

Lanari et al. (2023) found a correlation between Apennine drainage evolution, thermochronometric cooling ages and Moho geometry, suggesting an onset of slab break-off at the boundary between the northern and central Apennines and progressive southward migration of break-off through time. The distribution of earthquakes on the peri-Adriatic side of the Apennines suggests a clear boundary between a northern seismic zone and a southern zone with very few recorded earthquakes, potentially marking the northern limit of the break-off (Figure 8a). This limit approximately coincides with the locus of onset of southward migration of the Quaternary uplift pulse (Figure 8) and the region of the Apennines with the greatest cumulative uplift (Figure 10a). Rapid uplift recorded in northern Calabria since around 0.4 Ma (Olivetti et al., 2012), likely supported by mantle upwelling (Faccenna et al., 2011), could indicate the arrival of the slab window in the southern part of the Italian Peninsula. Combining this age with the onset of slab break-off in the central Apennines at ∼3 Ma, a propagation velocity of approximately 155 km/Myr over a distance of 400 km can be estimated (Figure 10b). The propagation rate suggested by the uplift acceleration model (∼90 km/Myr for the variable-K model, Figure 8f) is just over half of this, but is in the range of numerical modeling results for break-off of a relatively strong slab (van Hunen & Allen, 2011). Moreover, the part of the model showing temporal migration of uplift is less than 100 km long, and at the southern boundary of the model domain, only one channel (26) is sufficiently long to provide a clear history of rock uplift prior to ∼1 Ma. Additionally, the propagation rate of 155 km/Myr inferred above is an average of the entire break-off zone, but we do not know if the propagation rate was constant through time; it is possible that the lateral rupture rate may accelerate during the progression of slab rupture (e.g., van Hunen & Allen, 2011). Notwithstanding these complexities, the rock-uplift model we present provides new insights into the Quaternary rock-uplift history of the Apennine belt, which can be divided into three main stages (Figure 10b): (a) initially, spatially uniform rock-uplift rates are likely driven by slab rollback and the start of slab break-off beneath the central Apennines around 3.0–2.5 Ma; (b) rapid rock uplift between 2.5 and 1.5 Ma, producing rapid topographic growth in the central Apennines, followed the development of the slab window and the southward migration of break-off beneath the central belt; and (c) during the Middle Pleistocene, the break-off reached the Calabrian Peninsula and the subducting Adria slab attained its present configuration.

While the rapid rock-uplift pulse between 2.5 and 1.5 Ma may be associated with propagation of slab break-off, this mechanism does not explain the accelerated Middle Pleistocene to present-day rock uplift. This younger phase initiates nearly simultaneously across the entire study area, as indicated by both the variable-K rock-uplift model (Figure 8e) and the increase in river incision rates from the late Pleistocene to the Holocene (Figure 9) throughout the study area. Similar increases have been observed in the Basilicata (Southern Apennine, Gioia et al., 2024), the northern Calabrian coasts (Liberatore et al., 2023), and even in the Apulian peninsula, situated in the Apennine foreland and not directly involved in the building of the mountain chain (De Santis et al., 2021, 2023; Doglioni et al., 1994). No mechanism has yet been proposed to explain this recent uplift acceleration, and further studies are needed to investigate this phenomenon as well as the robustness of the short-versus long-term incision-rate estimates (e.g., Finnegan et al., 2014; Gallen et al., 2015).

6. Conclusions

In this study, we aimed to unravel the relationship between Quaternary rock uplift and the driving mechanisms that shaped the topography of the Apennine belt. By linearly inverting river profiles draining the Adriatic flank of the range with temporal calibration based on published denudation and incision-rate data, we obtained new insights into the rock-uplift history of the region. The approach of using a variable K value, applied to geological domains (mountain and coastal) that show different lithological and morphological characteristics, allowed us to

obtain temporal constraints on uplift histories that align well with independent chronological constraints on the different phases of mountain and coastal uplift and exhumation during the Quaternary.

The spatiotemporal rock-uplift model that we present provides new insights into the rates, timing, and pattern of Quaternary uplift on the northeastern side of the central Apennines. Our results suggest that rock uplift did not occur uniformly along the entire Apennine belt around 2.5 Ma but rather migrated southeastward through time, originating from the region that currently marks the boundary between the seismic northern peri-Adriatic belt and the seismically nearly inactive southern belt. Combining the inferred rock-uplift trend with tomographic data of the Adria slab, we argue that the mechanism responsible for the Quaternary uplift pulse is break-off of the Adria slab and southward propagation of the slab window over time. The most rapid rock-uplift rates, occurring between 2.5 and 1.5 Ma, resulted from the opening of a wide slab window in the area where the Apennines currently exhibit the highest elevations. Furthermore, our uplift model suggests a renewed acceleration in rock-uplift rates along the entire Adriatic coast from the Middle Pleistocene to the Holocene, coeval with acceleration of uplift in the eastern coast of Southern Italy and in the Apulian foreland. This recent uplift acceleration affecting such a wide area represents a new feature that appears unrelated to slab break-off propagation and requires further studies to test if it is real, and if so, to uncover its driving mechanism.

Conflict of Interest

The authors declare no conflicts of interest relevant to this study.

Data Availability Statement

The original code developed to perform linear river-profile inversion for variable erodibility can be found in the Supplementary material of Pazzaglia and Fisher (2022) and in the Zenodo repository provided by Fisher, Gallen, and Pazzaglia (2022). The modified version of the code used for this work is provided in the supplementary material.

Acknowledgments
We thank Boris Kaus for efficient editorial handling, and Frank Pazzaglia and an anonymous reviewer for insightful reviews that improved the quality of this manuscript. Open access funding enabled and organized by Projekt DEAL.

References

Amato, V., Aucelli, P. P. C., Bracone, V., Cesarano, M., & Rosskopf, C. M. (2017). Long-term landscape evolution of the Molise sector of the central-southern Apennines, Italy. *Geologica Carpathica*, *68*(1), 29–42. https://doi.org/10.1515/geoca-2017-0003

Artoni, A. (2007). Growth rates and two-mode accretion in the outer orogenic wedge-foreland basin system of Central Apennine (Italy). *Bolletino della Società Geolica Italiana*, *126*(3), 531–556.

Ballato, P., Landgraf, A., Schildgen, T. F., Stockli, D. F., Fox, M., Ghassemi, M. R., et al. (2015). The growth of a mountain belt forced by base-level fall: Tectonics and surface processes during the evolution of the Alborz Mountains, N Iran. *Earth and Planetary Science Letters*, *425*, 204–218. https://doi.org/10.1016/j.epsl.2015.05.051

Bartolini, C. (2003). When did the Northern Apennine become a mountain chain? *Quaternary International*, *101–102*, 75–80. https://doi.org/10.1016/S1040-6182(02)00090-3

Boccaletti, M., Corti, G., & Martelli, L. (2011). Recent and active tectonics of the external zone of the Northern Apennines (Italy). *International Journal of Earth Sciences*, *100*(6), 1331–1348. https://doi.org/10.1007/s00531-010-0545-y

Bosi, C., Galadini, F., Giaccio, B., Messina, P., & Sposato, A. (2003). Plio-Quaternary continental deposits in the Latium-Abruzzi Apennines: The correlation of geological events across different intermontane basins. *Italian Journal of Quaternary Sciences*, *16*, 55–76.

Braun, J. (2010). The many surface expressions of mantle dynamics. *Nature Geoscience*, *3*(12), 825–833. https://doi.org/10.1038/ngeo1020

Buccolini, M., Gentili, B., Materazzi, M., & Piacentini, T. (2010). Late Quaternary geomorphological evolution and erosion rates in the clayey peri-Adriatic belt (central Italy). *Geomorphology*, *116*(1), 145–161. https://doi.org/10.1016/j.geomorph.2009.10.015

Buleo Tebar, V., Bonasera, M., Racano, S., & Fubelli, G. (2024). River linear inversion to assess drainage base-level fall history in North-western Apennines and implications on the Alessandria Basin tectonic activity. *Geomorphology*, 109327. https://doi.org/10.1016/j.geomorph.2024.109327

Campforts, B., Schwanghart, W., & Govers, G. (2017). Accurate simulation of transient landscape evolution by eliminating numerical diffusion: The TTLEM 1.0 model. *Earth Surface Dynamics*, *5*(1), 47–66. https://doi.org/10.5194/esurf-5-47-2017

Carmignani, L., Decandia, F. A., Fantozzi, P. L., Lazzarotto, A., Liotta, D., & Meccheri, M. (1994). Tertiary extensional tectonics in Tuscany (Northern Apennines, Italy). *Tectonophysics*, *238*(1), 295–315. https://doi.org/10.1016/0040-1951(94)90061-2

Carminati, E., Lustrino, M., Cuffaro, M., & Doglioni, C. (2010). Tectonics, magmatism and geodynamics of Italy: What we know and what we imagine. *Journal of the Virtual Explorer*, *36*, 1–62. https://doi.org/10.3809/jvirtex.2010.00226

Carminati, E., Negredo, A. M., Valera, J. L., & Doglioni, C. (2005). Subduction-related intermediate-depth and deep seismicity in Italy: Insights from thermal and rheological modelling. *Physics of the Earth and Planetary Interiors*, *149*(1), 65–79. https://doi.org/10.1016/j.pepi.2004.04.006

Casero, P. (2004). Structural setting of petroleum exploration plays in Italy. *Special Volume of the Italian Geological Society for the IGC*, *32*, 189–199.

Cavinato, G. P., & De Celles, P. G. (1999). Extensional basins in the tectonically bimodal central Apennines fold-thrust belt, Italy: Response to corner flow above a subducting slab in retrograde motion. *Geology*, *27*(10), 955–958. https://doi.org/10.1130/0091-7613(1999)027<0955:EBITTB>2.3.CO;2

Centamore, E., Crescenti, U., Dramis, F., Bigi, S., Morelli, C., Coltorti, M., et al. (2006). Note Illustrative della Carta Geologica d'Italia alla scala 1:50.000. Foglio 360 TORRE DE' PASSERI, SE.L.CA. s.r.l.

Centamore, E., Crescenti, U., Dramis, F., Boncio, P., Lavecchia, G., Fumanti, F., et al. (2006). Note Illustrative della Carta Geologica d'Italia alla scala 1:50.000. Foglio 368 AVEZZANO, SE.L.CA. s.r.l.

Centamore, E., & Nisio, S. (2003). Effects of uplift and tilting in the Central-Northern Apennines (Italy). *Quaternary International*, *101–102*, 93–101. https://doi.org/10.1016/S1040-6182(02)00092-7

Centamore, E., & Rossi, D. (2009). Neogene-Quaternary tectonics and sedimentation in the Central Apennines. *Italian Journal of Geosciences*, *128*(1), 73–88.

Chiarabba, C., Bagh, S., Bianchi, I., De Gori, P., & Barchi, M. (2010). Deep structural heterogeneities and the tectonic evolution of the Abruzzi region (Central Apennines, Italy) revealed by microseismicity, seismic tomography, and teleseismic receiver functions. *Earth and Planetary Science Letters*, *295*(3), 462–476. https://doi.org/10.1016/j.epsl.2010.04.028

Chiarabba, C., Bianchi, I., De Gori, P., & Agostinetti, N. P. (2020). Mantle upwelling beneath the Apennines identified by receiver function imaging. *Scientific Reports*, *10*(1), 19760. https://doi.org/10.1038/s41598-020-76515-2

Chiarabba, C., Giacomuzzi, G., Bianchi, I., Agostinetti, N. P., & Park, J. (2014). From underplating to delamination-retreat in the northern Apennines. *Earth and Planetary Science Letters*, *403*, 108–116. https://doi.org/10.1016/j.epsl.2014.06.041

Chiarabba, C., Jovane, L., & DiStefano, R. (2005). A new view of Italian seismicity using 20 years of instrumental recordings. *Tectonophysics*, *395*(3), 251–268. https://doi.org/10.1016/j.tecto.2004.09.013

Clementucci, R., Ballato, P., Siame, L. L., Faccenna, C., Racano, S., Torreti, G., et al. (2023). Transient response to changes in uplift rates in the northern Atlas-Meseta system (Morocco). *Geomorphology*, *436*, 108765. https://doi.org/10.1016/j.geomorph.2023.108765

Codilean, A. T., Munack, H., Saktura, W. M., Cohen, T. J., Jacobs, Z., Ulm, S., et al. (2022). OCTOPUS database (v.2). *Earth System Science Data*, *14*(8), 3695–3713. https://doi.org/10.5194/essd-14-3695-2022

Collettini, C., & Barchi, M. R. (2004). A comparison of structural data and seismic images for low-angle normal faults in the Northern Apennines (Central Italy): Constraints on activity. *Geological Society, London, Special Publications*, *224*(1), 95–112. https://doi.org/10.1144/GSL.SP.2004.224.01.07

Collettini, C., De Paola, N., Holdsworth, R. E., & Barchi, M. R. (2006). The development and behaviour of low-angle normal faults during Cenozoic asymmetric extension in the Northern Apennines, Italy. *Journal of Structural Geology*, *28*(2), 333–352. https://doi.org/10.1016/j.jsg.2005.10.003

Cosentino, D., Asti, R., Nocentini, M., Gliozzi, E., Kotsakis, T., Mattei, M., et al. (2017). New insights into the onset and evolution of the central Apennine extensional intermontane basins based on the tectonically active L'Aquila Basin (central Italy). *Geological Society of America Bulletin*, *129*(9–10), 1314–1336. https://doi.org/10.1130/B31679.1

Cosentino, D., Cipollari, P., Marsili, P., & Scrocca, D. (2010). Geology of the central Apennines: A regional review. *Journal of the Virtual Explorer*, *36*(11), 1–37. https://doi.org/10.3809/jvirtex.2010.00223

Crescenti, U., Biondi, R., Boncio, P., Calamita, F., Miccadei, E., Pizzi, A., et al. (2015). Note Illustrative della Carta Geologica d'Italia alla scala 1:50.000. Foglio 361 CHIETI, SE.L.CA. s.r.l.

Cyr, A. J., & Granger, D. E. (2008). Dynamic equilibrium among erosion, river incision, and coastal uplift in the northern and central Apennines, Italy. *Geology*, *36*(2), 103–106. https://doi.org/10.1130/G24003A.1

Cyr, A. J., Granger, D. E., Olivetti, V., & Molin, P. (2014). Distinguishing between tectonic and lithologic controls on bedrock channel longitudinal profiles using cosmogenic ^{10}Be erosion rates and channel steepness index. *Geomorphology*, *209*, 27–38. https://doi.org/10.1016/j.geomorph.2013.12.010

D'Agostino, N., Jackson, J. A., Dramis, F., & Funiciello, R. (2001). Interactions between mantle upwelling, drainage evolution and active normal faulting: An example from the central Apennines (Italy). *Geophysical Journal International*, *147*(2), 475–497. https://doi.org/10.1046/j.1365-246X.2001.00539.x

D'Agostino, N., Mantenuto, S., D'Anastasio, E., Giuliani, R., Mattone, M., Calcaterra, S., et al. (2011). Evidence for localized active extension in the central Apennines (Italy) from global positioning system observations. *Geology*, *39*(4), 291–294. https://doi.org/10.1130/G31796.1

D'Anastasio, E., De Martini, P. M., Selvaggi, G., Pantosti, D., Marchioni, A., & Maseroli, R. (2006). Short-term vertical velocity field in the Apennines (Italy) revealed by geodetic levelling data. *Tectonophysics*, *418*(3), 219–234. https://doi.org/10.1016/j.tecto.2006.02.008

Delchiaro, M., Iacobucci, G., Della Seta, M., Gribenski, N., Piacentini, D., Ruscitto, V., et al. (2024). A fluvial record of late Quaternary climate changes and tectonic uplift along the Marche Piedmont Zone of the Apennines: New insights from the Tesino River (Italy). *Geomorphology*, *445*, 108971. https://doi.org/10.1016/j.geomorph.2023.108971

De Santis, V., Scardino, G., Meschis, M., Ortiz, J. E., Sánchez-Palencia, Y., & Caldara, M. (2021). Refining the middle-late Pleistocene chronology of marine terraces and uplift history in a sector of the Apulian foreland (southern Italy) by applying a synchronous correlation technique and amino acid racemization to Patella spp. and Thetystrombus latus. *Italian Journal of Geosciences*, *140*(3), 438–463. https://doi.org/10.3301/IJG.2021.05

De Santis, V., Scardino, G., Scicchitano, G., Meschis, M., Montagna, P., Pons-Branchu, E., et al. (2023). Middle-late Pleistocene chronology of palaeoshorelines and uplift history in the low-rising to stable Apulian foreland: Overprinting and reoccupation. *Geomorphology*, *421*, 108530. https://doi.org/10.1016/j.geomorph.2022.108530

Diaferia, G., Cammarano, F., & Faccenna, C. (2019). Thermal structure of a vanishing subduction system: An example of seismically-derived crustal temperature along the Italian peninsula. *Geophysical Journal International*, *219*(1), 239–247. https://doi.org/10.1093/gji/ggz289

Di Giulio, A., Mancin, N., Martelli, L., & Sani, F. (2013). Foredeep palaeobathymetry and subsidence trends during advancing then retreating subduction: The Northern Apennine case (Oligocene-Miocene, Italy). *Basin Research*, *25*(3), 260–284. https://doi.org/10.1111/bre.12002

Doglioni, C., Mongelli, F., & Pieri, P. (1994). The Puglia uplift (SE Italy): An anomaly in the foreland of the Apenninic subduction due to buckling of a thick continental lithosphere. *Tectonics*, *13*(5), 1309–1321. https://doi.org/10.1029/94TC01501

Duretz, T., & Gerya, T. V. (2013). Slab detachment during continental collision: Influence of crustal rheology and interaction with lithospheric delamination. *Tectonophysics*, *602*, 124–140. https://doi.org/10.1016/j.tecto.2012.12.024

Eva, E., Ferretti, G., & Solarino, S. (2005). Superposition of different stress orientations in the western sector of the northern Apennines (Italy). *Journal of Seismology*, *9*(4), 413–430. https://doi.org/10.1007/s10950-005-1419-9

Faccenna, C., & Becker, T. W. (2020). Topographic expressions of mantle dynamics in the Mediterranean. *Earth-Science Reviews*, *209*, 103327. https://doi.org/10.1016/j.earscirev.2020.103327

Faccenna, C., Becker, T. W., Miller, M. S., Serpelloni, E., & Willett, S. D. (2014). Isostasy, dynamic topography, and the elevation of the Apennines of Italy. *Earth and Planetary Science Letters*, *407*, 163–174. https://doi.org/10.1016/j.epsl.2014.09.027

Faccenna, C., Funiciello, F., Civetta, L., D'Antonio, M., Moroni, M., & Piromallo, C. (2007). Slab disruption, mantle circulation, and the opening of the Tyrrhenian basins. In L. Beccaluva, G. Bianchini, & M. Wilson (Eds.), *Cenozoic volcanism in the Mediterranean area* (Vol. 418, pp. 153–170). Geological Society of America Special Paper. https://doi.org/10.1130/2007.2418(08)

Faccenna, C., Molin, P., Orecchio, B., Olivetti, V., Bellier, O., Funiciello, F., et al. (2011). Topography of the Calabria subduction zone (southern Italy): Clues for the origin of Mt. Etna. *Tectonics*, *30*(1), TC1003. https://doi.org/10.1029/2010TC002694

Faccenna, C., Piromallo, C., Crespo-Blanc, A., Jolivet, L., & Rossetti, F. (2004). Lateral slab deformation and the origin of the western Mediterranean arcs. *Tectonics*, *23*(1), TC1012. https://doi.org/10.1029/2002TC001488

Faure Walker, J. P., Roberts, G. P., Cowie, P. A., Papanikolaou, I., Michetti, A. M., Sammonds, P., et al. (2012). Relationship between topography, rates of extension and mantle dynamics in the actively-extending Italian Apennines. *Earth and Planetary Science Letters*, *325–326*, 76–84. https://doi.org/10.1016/j.epsl.2012.01.028

Fellin, M. G., San Jose, M., Faccenna, C., Willett, S. D., Cosentino, D., Lanari, R., et al. (2021). Transition from slab roll-back to slab break-off in the central Apennines, Italy: Constraints from the stratigraphic and thermochronologic record. *Geological Society of America Bulletin*, *134*(7–8), 1916–1930. https://doi.org/10.1130/B36123.1

Finnegan, N. J., Schumer, R., & Finnegan, S. (2014). A signature of transience in bedrock river incision rates over timescales of 10^4–10^7 years. *Nature*, *505*(7483), 391–394. https://doi.org/10.1038/nature12913

Fisher, J., Gallen, S. J., & Pazzaglia, F. J. (2022). jamesfisher-gis/LongProfileLinearInversion: Linear Inversion of River Longitudinal Profile v1.2 (v1.2). *Zenodo*. https://doi.org/10.5281/zenodo.6503006

Fisher, J. A., Pazzaglia, F. J., Anastasio, D. J., & Gallen, S. F. (2022). Linear inversion of fluvial topography in the northern Apennines: Comparison of base-level fall to crustal shortening. *Tectonics*, *41*(11), e2022TC007379. https://doi.org/10.1029/2022TC007379

Fox, M., Leith, K., Bodin, T., Balco, G., & Shuster, D. L. (2015). Rate of fluvial incision in the Central Alps constrained through joint inversion of detrital ^{10}Be and thermochronometric data. *Earth and Planetary Science Letters*, *411*, 27–36. https://doi.org/10.1016/j.epsl.2014.11.038

Funiciello, R., Giordano, G., & De Rita, D. (2003). The Albano maar lake (Colli Albani Volcano, Italy): Recent volcanic activity and evidence of pre-Roman age catastrophic lahar events. *Journal of Volcanology and Geothermal Research*, *123*(1), 43–61. https://doi.org/10.1016/S0377-0273(03)00027-1

Gailleton, B., Mudd, S. M., Clubb, F. J., Grieve, S. W. D., & Hurst, M. D. (2021). Impact of changing concavity indices on channel steepness and divide migration metrics. *Journal of Geophysical Research: Earth Surface*, *126*(10), e2020JF006060. https://doi.org/10.1029/2020JF006060

Galadini, F., Messina, P., Giaccio, B., & Sposato, A. (2003). Early uplift history of the Abruzzi Apennines (central Italy): Available geomorphological constraints. *Quaternary International*, *101–102*, 125–135. https://doi.org/10.1016/S1040-6182(02)00095-2

Gallen, S. F. (2018). Lithologic controls on landscape dynamics and aquatic species evolution in post-orogenic mountains. *Earth and Planetary Science Letters*, *493*, 150–160. https://doi.org/10.1016/j.epsl.2018.04.029

Gallen, S. F., Pazzaglia, F. J., Wegmann, K. W., Pederson, J. L., & Gardner, T. W. (2015). The dynamic reference frame of rivers and apparent transience in incision rates. *Geology*, *43*(7), 623–626. https://doi.org/10.1130/g36692.1

Gallen, S. F., Seymour, N. M., Glotzbach, C., Stockli, D. F., & O'Sullivan, P. (2023). Calabrian forearc uplift paced by slab–mantle interactions during subduction retreat. *Nature Geoscience*, *16*(6), 513–520. https://doi.org/10.1038/s41561-023-01185-4

Giachetta, E., & Willett, S. D. (2018). Effects of river capture and sediment flux on the evolution of plateaus: Insights from numerical modeling and river profile analysis in the Upper Blue Nile Catchment. *Journal of Geophysical Research: Earth Surface*, *123*(6), 1187–1217. https://doi.org/10.1029/2017JF004252

Giacomuzzi, G., Civalleri, M., De Gori, P., & Chiarabba, C. (2012). A 3D Vs model of the upper mantle beneath Italy: Insight on the geodynamics of central Mediterranean. *Earth and Planetary Science Letters*, *335–336*, 105–120. https://doi.org/10.1016/j.epsl.2012.05.004

Gioia, D., Corrado, G., Minervino Amodio, A., & Schiattarella, M. (2024). Uplift rate calculation based on the comparison between marine terrace data and river profile analysis: A morphotectonic insight from the Ionian coastal belt of Basilicata, Italy. *Geomorphology*, *447*, 109030. https://doi.org/10.1016/j.geomorph.2023.109030

Glotzbach, C. (2015). Deriving rock uplift histories from data-driven inversion of river profiles. *Geology*, *43*(6), 467–470. https://doi.org/10.1130/G36702.1

Gong, L., van der Beek, P., Schildgen, T. F., Sobel, E. R., Racano, S., & Mariotti, A. (2024). Drainage rearrangement in an intra-continental mountain belt: A case study from the central South Tian Shan, Kyrgyzstan [preprint]. *EGUsphere*. https://doi.org/10.5194/egusphere-2023-2651

Goren, L., Fox, M., & Willett, S. D. (2014). Tectonics from fluvial topography using formal linear inversion: Theory and applications to the Inyo Mountains, California. *Journal of Geophysical Research: Earth Surface*, *119*(8), 1651–1681. https://doi.org/10.1002/2014JF003079

Gvirtzman, Z., & Nur, A. (2001). Residual topography, lithospheric structure and sunken slabs in the central Mediterranean. *Earth and Planetary Science Letters*, *187*(1–2), 117–130. https://doi.org/10.1016/S0012-821X(01)00272-2

Howard, A. D. (1994). A detachment-limited model of drainage basin evolution. *Water Resources Research*, *30*(7), 2261–2285. https://doi.org/10.1029/94WR00757

Lanari, R., Reitano, R., Faccenna, C., Agostinetti, N. P., & Ballato, P. (2023). Surface and crustal response to deep subduction dynamics: Insights from the Apennines, Italy. *Tectonics*, *42*(3), e2022TC007461. https://doi.org/10.1029/2022TC007461

Liberatore, M., Gliozzi, E., Cipollari, P., & Cosentino, D. (2023). Holocene vertical velocity fields in the Calabrian Arc (southern Italy): New insights from uplifted sea-level markers in the Crotone Peninsula. *Quaternary Science Reviews*, *321*, 108368. https://doi.org/10.1016/j.quascirev.2023.108368

Magni, V., Allen, M. B., van Hunen, J., & Bouilhol, P. (2017). Continental underplating after slab break-off. *Earth and Planetary Science Letters*, *474*, 59–67. https://doi.org/10.1016/j.epsl.2017.06.017

McNab, F., Ball, P. W., Hoggard, M. J., & White, N. J. (2018). Neogene uplift and magmatism of Anatolia: Insights from drainage analysis and basaltic geochemistry. *Geochemistry, Geophysics, Geosystems*, *19*(1), 175–213. https://doi.org/10.1002/2017GC007251

Molin, P., & Fubelli, G. (2005). Morphometric evidence of the topographic growth of central Apennines. *Geografia Fisica e Dinamica Quaternaria*, *28*, 47–61.

Molin, P., Fubelli, G., Nocentini, M., Sperini, S., Ignat, P., Grecu, F., & Dramis, F. (2012). Interaction of mantle dynamics, crustal tectonics, and surface processes in the topography of the Romanian Carpathians: A geomorphological approach. *Global and Planetary Change*, *90*(91), 58–72. https://doi.org/10.1016/j.gloplacha.2011.05.005

Molin, P., Sembroni, A., Ballato, P., & Faccenna, C. (2023). The uplift of an early stage collisional plateau unraveled by fluvial network analysis and river longitudinal profile inversion: The case of the Eastern Anatolian Plateau. *Tectonics*, *42*(8), e2022TC007737. https://doi.org/10.1029/2022TC007737

Montone, P., Amato, A., & Pondrelli, S. (1999). Active stress map of Italy. *Journal of Geophysical Research*, *104*(B11), 25595–25610. https://doi.org/10.1029/1999JB900181

Montone, P., Mariucci, M. T., & Pierdominici, S. (2012). The Italian present-day stress map. *Geophysical Journal International*, *189*(2), 705–716. https://doi.org/10.1111/j.1365-246X.2012.05391.x

Montone, P., Mariucci, M. T., Pondrelli, S., & Amato, A. (2004). An improved stress map for Italy and surrounding regions (central Mediterranean). *Journal of Geophysical Research*, *109*(B10), B10410. https://doi.org/10.1029/2003JB002703

Mudd, S. M., Harel, M.-A., Hurst, M. D., Grieve, S. W. D., & Marrero, S. M. (2016). The CAIRN method: Automated, reproducible calculation of catchment-averaged denudation rates from cosmogenic nuclide concentrations. *Earth Surface Dynamics*, *4*(3), 655–674. https://doi.org/10.5194/esurf-4-655-2016

Olivetti, V., Cyr, A. J., Molin, P., Faccenna, C., & Granger, D. E. (2012). Uplift history of the Sila Massif, southern Italy, deciphered from cosmogenic ^{10}Be erosion rates and river longitudinal profile analysis. *Tectonics*, *31*(3), TC3007. https://doi.org/10.1029/2011TC003037

Ott, R. F., Gallen, S. F., Caves Rugenstein, J. K., Ivy-Ochs, S., Helman, D., Fassoulas, C., et al. (2019). Chemical versus mechanical denudation in meta-clastic and carbonate bedrock catchments on Crete, Greece, and mechanisms for steep and high carbonate topography. *Journal of Geophysical Research: Earth Surface*, *124*(12), 2943–2961. https://doi.org/10.1029/2019jf005142

Pan, R., Han, Z., Su, Q., Li, G., Li, X., Li, Y., & Wang, X. (2023). Two-staged uplift of the southeast margin of the Tibetan plateau revealed by river longitudinal profiles. *Frontiers in Earth Science*, *11*, 1124362. https://doi.org/10.3389/feart.2023.1124362

Pandeli, E., Bartolini, C., Dini, A., & Antolini, E. (2009). New data on the paleogeography of Southern Tuscany (Italy) since Late Miocene. *International Journal of Earth Sciences*, *99*(6), 1357–1381. https://doi.org/10.1007/s00531-009-0463-z

Patacca, E., Sartori, R., & Scandone, P. (1993). Tyrrhenian Basin and Apennines. Kinematic evolution and related dynamic constraints. In E. Boschi, E. Mantovani, & A. Morelli (Eds.), *Recent evolution and seismicity of the Mediterranean region* (pp. 161–171). Springer Netherlands. https://doi.org/10.1007/978-94-011-2016-6_7

Pavano, F., & Gallen, S. F. (2021). A geomorphic examination of the Calabrian forearc translation. *Tectonics*, *40*(7), e2020TC006692. https://doi.org/10.1029/2020TC006692

Pavano, F., Pazzaglia, F. J., Rittenour, T. M., Catalano, S., Corbett, L. B., & Bierman, P. (2024). Integrated uplift, subsidence, erosion and deposition in a tightly coupled source-to-sink system, Pagliara basin, northeastern Sicily, Italy. *Basin Research*, *36*(1), e12845. https://doi.org/10.1111/bre.12845

Pazzaglia, F. J., & Fisher, J. A. (2022). A reconstruction of Apennine uplift history and the development of transverse drainages from longitudinal profile inversion. In C. Koeberl, P. Claeys, & A. Montanari (Eds.), *From the Guajira Desert to the Apennines, and from Mediterranean Microplates to the Mexican Killer Asteroid: Honoring the Career of Walter Alvarez* (Vol. 557, pp. 129–148). Geological Society of America Special Paper. https://doi.org/10.1130/2022.2557(09)

Perron, J. T., & Royden, L. (2013). An integral approach to bedrock river profile analysis. *Earth Surface Processes and Landforms*, *38*(6), 570–576. https://doi.org/10.1002/esp.3302

Picotti, V., & Pazzaglia, F. J. (2008). A new active tectonic model for the construction of the Northern Apennines mountain front near Bologna (Italy). *Journal of Geophysical Research*, *113*(B8), B08412. https://doi.org/10.1029/2007JB005307

Pieruccini, P., Celma, C. D., Rita, F. D., Magri, D., Carnevale, G., Farabollini, P., et al. (2016). Sedimentology, faunal content and pollen record of Middle Pleistocene palustrine and lagoonal sediments from the Peri-Adriatic basin, Abruzzi, eastern central Italy. *Quaternary Research*, *86*(3), 359–372. https://doi.org/10.1016/j.yqres.2016.08.003

Piromallo, C., & Morelli, A. (2003). P wave tomography of the mantle under the Alpine-Mediterranean area. *Journal of Geophysical Research*, *108*(B2), 2065. https://doi.org/10.1029/2002JB001757

Pizzi, A. (2003). Plio-Quaternary uplift rates in the outer zone of the central Apennines fold-and-thrust belt, Italy. *Quaternary International*, *101–102*, 229–237. https://doi.org/10.1016/S1040-6182(02)00105-2

Pritchard, D., Roberts, G. G., White, N. J., & Richardson, C. N. (2009). Uplift histories from river profiles. *Geophysical Research Letters*, *36*(24), L24301. https://doi.org/10.1029/2009GL040928

Quye-Sawyer, J., Whittaker, A. C., & Roberts, G. G. (2020). Calibrating fluvial erosion laws and quantifying river response to faulting in Sardinia, Italy. *Geomorphology*, *370*, 107388. https://doi.org/10.1016/j.geomorph.2020.107388

Racano, S., Schildgen, T., Ballato, P., Yıldırım, C., & Wittmann, H. (2023). Rock-uplift history of the Central Pontides from river-profile inversions and implications for development of the North Anatolian Fault. *Earth and Planetary Science Letters*, *616*, 118231. https://doi.org/10.1016/j.epsl.2023.118231

Racano, S., Schildgen, T. F., Cosentino, D., & Miller, S. R. (2021). Temporal and spatial variations in rock uplift from river-profile inversions at the Central Anatolian Plateau southern margin. *Journal of Geophysical Research: Earth Surface*, *126*(8), e2020JF006027. https://doi.org/10.1029/2020JF006027

Rohrmann, A., Kirby, E., & Schwanghart, W. (2023). Accelerated Miocene incision along the Yangtze River driven by headward drainage basin expansion. *Science Advances*, *9*(36), eadh1636. https://doi.org/10.1126/sciadv.adh1636

Royden, L., Patacca, E., & Scandone, P. (1987). Segmentation and configuration of subducted lithosphere in Italy: An important control on thrust-belt and foredeep-basin evolution. *Geology*, *15*(8), 714–717. https://doi.org/10.1130/0091-7613(1987)15<714:SACOSL>2.0.CO;2

San Jose, M., Caves Rugenstein, J. K., Cosentino, D., Faccenna, C., Fellin, M. G., Ghinassi, M., & Martini, I. (2020). Stable isotope evidence for rapid uplift of the central Apennines since the late Pliocene. *Earth and Planetary Science Letters*, *544*, 116376. https://doi.org/10.1016/j.epsl.2020.116376

Schildgen, T. F., Cosentino, D., Bookhagen, B., Niedermann, S., Yıldırım, C., Echtler, H., et al. (2012). Multi-phased uplift of the southern margin of the Central Anatolian plateau, Turkey: A record of tectonic and upper mantle processes. *Earth and Planetary Science Letters*, *317–318*, 85–95. https://doi.org/10.1016/j.epsl.2011.12.003

Schwanghart, W., & Scherler, D. (2014). Short Communication: TopoToolbox 2 – MATLAB-based software for topographic analysis and modeling in Earth surface sciences. *Earth Surface Dynamics*, *2*(1), 1–7. https://doi.org/10.5194/esurf-2-1-2014

Scrocca, D. (2006). Thrust front segmentation induced by differential slab retreat in the Apennines (Italy). *Terra Nova*, *18*(2), 154–161. https://doi.org/10.1111/j.1365-3121.2006.00675.x

Sembroni, A., Molin, P., Soligo, M., Tuccimei, P., Anzalone, E., Billi, A., et al. (2020). The uplift of the Adriatic flank of the Apennines since the Middle Pleistocene: New insights from the Tronto River basin and the Acquasanta Terme Travertine (central Italy). *Geomorphology*, *352*, 106990. https://doi.org/10.1016/j.geomorph.2019.106990

Serpelloni, E., Faccenna, C., Spada, G., Dong, D., & Williams, S. D. P. (2013). Vertical GPS ground motion rates in the Euro-Mediterranean region: New evidence of velocity gradients at different spatial scales along the Nubia-Eurasia plate boundary. *Journal of Geophysical Research: Solid Earth*, *118*(11), 6003–6024. https://doi.org/10.1002/2013JB010102

Siravo, G., Molin, P., Sembroni, A., Fellin, M. G., & Faccenna, C. (2021). Tectonically driven drainage reorganization in the Eastern Cordillera, Colombia. *Geomorphology*, *389*, 107847. https://doi.org/10.1016/j.geomorph.2021.107847

Smith, A. G. G., Fox, M., Schwanghart, W., & Carter, A. (2022). Comparing methods for calculating channel steepness index. *Earth-Science Reviews*, *227*, 103970. https://doi.org/10.1016/j.earscirev.2022.103970

Tentori, D., Marsaglia, K. M., & Milli, S. (2016). Sand compositional changes as a support for sequence-stratigraphic interpretation: The middle upper Pleistocene to Holocene deposits of the Roman Basin (Rome, Italy). *Journal of Sedimentary Research*, *86*(10), 1208–1227. https://doi.org/10.2110/jsr.2016.75

Tropeano, M., Sabato, L., & Pieri, P. (2002). Filling and cannibalization of a foredeep: The Bradanic Trough, Southern Italy. *Geological Society, London, Special Publications*, *191*(1), 55–79. https://doi.org/10.1144/GSL.SP.2002.191.01.05

van Hunen, J., & Allen, M. B. (2011). Continental collision and slab break-off: A comparison of 3-D numerical models with observations. *Earth and Planetary Science Letters*, *302*(1), 27–37. https://doi.org/10.1016/j.epsl.2010.11.035

von Blanckenburg, F. (2005). The control mechanisms of erosion and weathering at basin scale from cosmogenic nuclides in river sediment. *Earth and Planetary Science Letters*, *237*(3), 462–479. https://doi.org/10.1016/j.epsl.2005.06.030

Wegmann, K. W., & Pazzaglia, F. J. (2009). Late Quaternary fluvial terraces of the Romagna and Marche Apennines, Italy: Climatic, lithologic, and tectonic controls on terrace genesis in an active orogen. *Quaternary Science Reviews*, *28*(1–2), 137–165. https://doi.org/10.1016/j.quascirev.2008.10.006

Whipple, K. X. (2009). The influence of climate on the tectonic evolution of mountain belts. *Nature Geoscience*, *2*(2), 97–104. https://doi.org/10.1038/ngeo413

Whipple, K. X., & Tucker, G. E. (1999). Dynamics of the stream-power river incision model: Implications for height limits of mountain ranges, landscape response timescales, and research needs. *Journal of Geophysical Research*, *104*(B8), 17661–17674. https://doi.org/10.1029/1999JB900120

Wittmann, H., Malusà, M. G., Resentini, A., Garzanti, E., & Niedermann, S. (2016). The cosmogenic record of mountain erosion transmitted across a foreland basin: Source-to-sink analysis of in situ ^{10}Be, ^{26}Al and ^{21}Ne in sediment of the Po river catchment. *Earth and Planetary Science Letters*, *452*, 258–271. https://doi.org/10.1016/j.epsl.2016.07.017

Wobus, C., Whipple, K. X., Kirby, E., Snyder, N., Johnson, J., Spyropolou, K., et al. (2006). Tectonics from topography: Procedures, promise, and pitfalls. In S. D. Willett, N. Hovius, M. T. Brandon, & D. M. Fisher (Eds.), *Tectonics, climate, and landscape evolution* (Vol. 398, pp. 55–74). Geological Society of America Special Paper. https://doi.org/10.1130/2006.2398(04)

Wolf, S. G., Huismans, R. S., Braun, J., & Yuan, X. (2022). Topography of mountain belts controlled by rheology and surface processes. *Nature*, *606*(7914), 516–521. https://doi.org/10.1038/s41586-022-04700-6

Wortel, M. J. R., & Spakman, W. (2000). Subduction and slab detachment in the Mediterranean-Carpathian region. *Science*, *290*(5498), 1910–1917. https://doi.org/10.1126/science.290.5498.1910

York, D., Evensen, N. M., Martínez, M. L., & De Basabe Delgado, J. (2004). Unified equations for the slope, intercept, and standard errors of the best straight line. *American Journal of Physics*, *72*(3), 367–375. https://doi.org/10.1119/1.1632486

Zhong, Y., Willett, S. D., Picotti, V., Xiong, J., & Zhang, H. (2022). Spatial and temporal variations of incision rate of the middle Yellow River and its tributaries. *Journal of Geophysical Research: Earth Surface*, *127*(1), e2021JF006327. https://doi.org/10.1029/2021JF006327